HHS Public Access

Author manuscript

J Org Chem. Author manuscript; available in PMC 2024 May 19.

Published in final edited form as:

J Org Chem. 2023 May 19; 88(10): 6509–6522. doi:10.1021/acs.joc.3c00191.

Hybrid Catalysts for Enantioselective Photo-Phosphoric Acid Catalysis

Alessa B. Rolka,
Institute of Organic Chemistry, Faculty of Chemistry and Pharmacy, University of Regensburg, D-93040 Regensburg, Germany; Department of Chemistry, University of California, Berkeley, California 94720, United States

Nataliya Archipowa,
Institute of Biophysics and Physical Biochemistry, Faculty of Biology and Preclinical Medicine, University of Regensburg, D-93040 Regensburg, Germany

Roger J. Kutta,
Institute of Theoretical and Physical Chemistry, Faculty of Chemistry and Pharmacy, University of Regensburg, D-93040 Regensburg, Germany

Burkhard König,
Institute of Organic Chemistry, Faculty of Chemistry and Pharmacy, University of Regensburg, D-93040 Regensburg, Germany

F. Dean Toste
Department of Chemistry, University of California, Berkeley, California 94720, United States

Abstract

The syntheses of two novel, organic, and chiral photocatalysts are presented. By combining donor–acceptor cyanoarene-based photocatalysts with a chiral phosphoric acid, bifunctional catalysts have been designed. In preliminary proof-of-concept reactions, their use in both enantioselective energy transfer and photoredox catalysis is demonstrated.

Graphical Abstract

Corresponding Authors Burkhard König – Burkhard.koenig@chemie.uni-regensburg.de, **F. Dean Toste** – fdtoste@berkeley.edu.

ASSOCIATED CONTENT

Supporting Information

The Supporting Information is available free of charge at https://pubs.acs.org/doi/10.1021/acs.joc.3c00191.

Photophysical measurements; CV data; overview schemes of photocatalyst synthesis; synthesis of literature known compounds; synthesis of PCII-Cl intermediate; HPLC spectra; NMR spectra (PDF)

Complete contact information is available at: https://pubs.acs.org/10.1021/acs.joc.3c00191

The authors declare no competing financial interest.

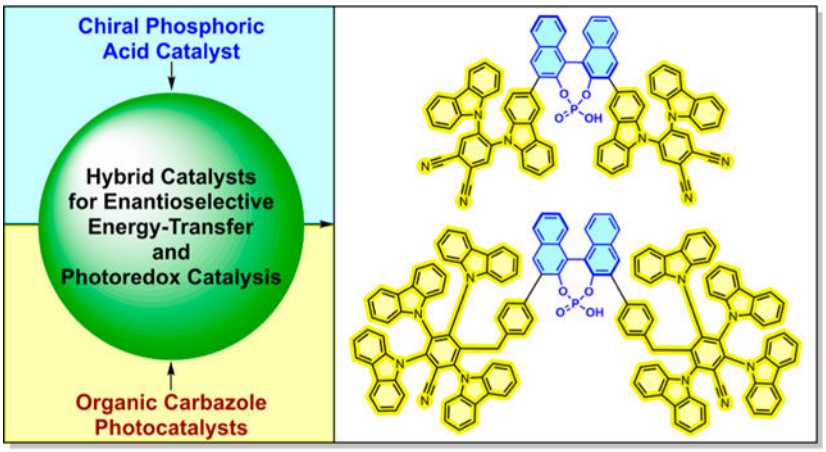

INTRODUCTION

Within the rapidly expanding field of photocatalysis, the development of enantioselective transformations remains challenging due to the high reactivity and transient nature of photoexcited intermediates. A particular challenge in this area is the suppression of uncatalyzed background processes that give rise to undesired racemic products. To tackle this problem, creative strategies have been developed[1–3] such as utilizing chiral Lewis acid catalysis in conjuncture with a separate photocatalyst or via direct excitation of the substrate. Within these strategies, the role of the chiral Lewis acid for the enantioselectivity of the photocatalyzed reaction can be manifold as has been elegantly shown by pioneering work of the groups of Bach,[4] Yoon,[5] and Meggers.[6]

One such mode of enantioinduction via a chiral Lewis acid was shown by the Bach group in the [2 + 2] photocycloaddition of enones (Scheme 1A).[4e] In this example, coordination of chiral Lewis acid **LA1** to the substrate results in a red-shifted absorption of the substrate by lowering the energy of the LUMO, rendering an uncoordinated racemic background reaction less feasible as compared to excitation of the chiral Lewis acid substrate complex. While this strategy relies on direct excitation of the substrate, the work of Yoon introduced the use of a chiral Lewis acid for enantioselective triplet energy-transfer catalysis that proceeds with a discrete photocatalyst separate from the Lewis acid (Scheme 1B).[5c] In this case, the coordination of the chiral Lewis acid complex to 2′-hydroxychalcones causes a significant lowering of the triplet energy of the substrate, allowing for selective excitation and subsequent enantioselective control.

In addition to utilizing Lewis acids to enable enantioselective photocatalytic processes, the use of hydrogen bonding as another secondary mode of catalysis is of particular importance in this field.[1b,3] This noncovalent interaction has been established as a powerful method to control the selectivity of photocatalytic transformations leading to the existence of a multitude of chiral catalysts containing a hydrogen bonding site. The first bifunctional hydrogen bonding photocatalyst for an intramolecular enantioselective [2 + 2] photocycloaddition of quinolones was introduced in 2003 by Krische et al. and utilized benzophenone as a sensitizing moiety (Figure 1).[7] While this example was important in

demonstrating the potential of enantioselective catalysis via sensitization by a photocatalyst with a pendant chiral motif, it suffers from relatively poor enantioselectivities. Since then, the Bach group has developed modified catalysts that result in higher selectivities, first by attaching a benzophenone photosensitizer to a lactam backbone and later by improving on this structure through the incorporation of a xanthone photosensitizer (xanthone catalyst shown in Scheme 2A).[3,8]

Despite the success of these catalysts in chiral photocatalysis, their ability to promote competing hydrogen atom abstraction reactions results in decomposition of the catalyst that limits their long-term stability. Further, both benzophenone and xanthone absorb light in the ultraviolet region, which often has sufficiently high energy to directly excite substrates, resulting in undesired background reactions. In 2014, the Bach group overcame this wavelength limitation by presenting the synthesis of a chiral thioxanthone, allowing for the use of visible light in an enantioselective [2 + 2] photocycloaddition (Scheme 2B).[9]

Building on the thioxanthone scaffold six years later, the group further enhanced its reactivity by combining this photocatalyst with a different hydrogen-bonding motif in the form of chiral phosphoric acids to yield novel bifunctional catalysts **TX-PA1** and **TX-PA2** (Scheme 2C).[10] Shortly thereafter, the group of Masson independently reported the synthesis of **TX-PA2** and its monosubstituted C_1-symmetric-derivate featuring only one thioxanthone moiety.[11f] The use of **TX-PA1** to promote enantioselective processes was demonstrated in a [2 + 2] intermolecular cycloaddition reaction with β-carboxyl-substituted cyclic enones. The chiral phosphoric acid moiety binds to the carboxylic acid by means of two hydrogen bonds, imprinting its chirality, while the attached thioxanthone moieties induce the energy transfer process. Enantiomeric ratios of up to 93:7 were achieved, albeit with only a relatively small substrate scope and with overall low yields. Despite the achievements of bifunctional thioxanthone-based catalysts in the field of enantioselective photocatalysis,[11] the ability to further modify the thioxanthone photocatalyst core of these chiral catalysts has proven to be limited and modifications are usually focusing on the attached chiral backbone, and not the photocatalyst itself. Consequently, addressing limitations of these chiral thioxanthone-photocatalysts, such as unmatched redox potentials or insufficient triplet energies, remains challenging.[12] For example, the triplet energy of modified thioxanthone based **TX-PA1** is significantly lowered as compared to the parent thioxanthen-9-one (from 272 to 235 kJ/mol). Hence, there is a need for bifunctional phosphoric acid photocatalysts with more readily tuned photophysical properties which inspired us to think about alternative catalyst structures that would allow for increased design flexibility.

Specifically, we were interested in the introduction of well-known donor–acceptor cyanoarene-based photocatalysts into the backbone of chiral phosphoric acids. We were especially attracted to this family of photocatalysts because of their extensively studied photophysical properties and their known understanding of how structural changes result in a tuning of these properties. This tuning is achieved by changing the nature of donors and acceptors, which in turn change the charge transfer characteristics of these photocatalysts and therefore impact their redox and photophysical properties.[13] Within this wide class of carbazole-based photocatalysts, we were particularly excited by the inexpensive organic dye **4CzIPN**, which has found tremendous applications in photocatalysis[14] since its introduction

in 2012 originally in the context of organic light-emitting diode (OLED) research.[15b] The widespread adoption of this catalyst is due to its promising photophysical properties, including a high photoluminescence quantum yield (up to 94.6%) and a long lifetime in the excited state. Additionally, the wide redox potential window, that is comparable to that of commonly utilized Ru- and Ir-polypyridyl catalysts, combined with a high chemical stability make this system a particularly attractive catalyst choice. Furthermore, carbazole-based photocatalysts have found utility as both effective photoredox catalysts as well as highly efficient energy transfer catalysts.[16,17] On the basis of these promising features, we hypothesized that novel chiral catalysts derived from the union of chiral phosphoric acids and donor–acceptor cyanoarene-based photocatalysts would open new chemical space in both enantioselective visible light-mediated photoredox and energy transfer catalysis.

SYNTHESIS AND CHALLENGES

For the reasons discussed above, we started our synthetic approach with the goal of attaching a **4CzIPN** derived moiety to a BINOL-based chiral phosphoric acid. We envisioned starting our synthesis of this new chiral photocatalyst from the literature reported chiral BINOL boronic acid 2 (Scheme 3A).[18,19]

From this intermediate, a Suzuki coupling with a brominated analogue **4** of **4CzIPN** was envisioned to allow for the desired union of the photocatalyst with the BINOL backbone of what will become the phosphoric acid.[19] Inspired by earlier reports from our group about photosubstitution reactions of the nitrile group at **4CzIPN** and **2CzPN**, we considered leveraging this photoredox radical coupling for the synthesis of the necessary brominated 4CzIPN derivative 4.[20] To our delight, the previously unreported reaction of **4CzIPN** (**3**) with 4-bromophenylacetic acid gave the desired product **4** without any detrimental effects due to the presence of the potentially reactive aryl bromide (Scheme 3B, second step). This functionalization reaction proceeded in good yield when performed on a small scale (60 μmol) using irradiation from below via a 451 nm LED plate through the bottom of 5 mL crimp cap vials; however, scaling up the reaction to a synthetically useful 2.4 mmol using a Kessil lamp (λ_{max} = 440 nm) yielded just 42% of the desired substrate after 1 h reaction time, in contrast to the 70% observed on the 60 μmol scale under otherwise identical conditions. By doubling the concentration and increasing the time to 5 h, a 72% isolated yield was achieved on a 2.4 mmol scale (Scheme 3B).

Next, the palladium cross-coupling of **4** and **2** was investigated (Table 1). Solubility issues of **4** in commonly used solvents for Suzuki coupling, such as 1,4 dioxane/water (entry 1), resulted in low yield; therefore, DMF was added as a third cosolvent (entry 2) to increase both solubility and yield. Using only a DMF/water mixture (entry 3) resulted in similar yields as 1,4-dioxane/water and provided worse results than the three-solvent system. Doubling the catalyst loading (entry 4) or increasing the equivalents of base (entry 5) did not have major impacts on the yield.

Testing different palladium sources (e.g., Pd(dppf)Cl_2·DCM) and different solvents (e.g., dichloroethane) also gave very low yields. Changing the base to sodium carbonate decreased the yield (entry 6), while using cesium carbonate in the solvent system gave the best result

with 45% isolated yield (entry 7) of the desired coupled product **5**. The remaining mass balance was attributed to the formation of monocoupled product **6** (26% isolated yield) and a mixture of starting material **4** and debrominated starting material. With sufficiently optimized conditions in hand, the Suzuki coupling was scaled up to 0.7 mmol of starting material **2** without significant impact on the yield (43% isolated yield).

Next, demethylation of **5** to produce the free binaphthol necessary for the introduction of the phosphoric acid was achieved by using BBr_3 (4.0 equiv, 1 M in DCM),[10,19] resulting in quantitative formation of **7** without the need for purification by column chromatography (Scheme 4, first step).

In the final step, the phosphoric acid moiety was introduced (Scheme 4, second step).[21] After purification via recrystallization induced selective precipitation of impurities from hot MeCN followed by column chromatography, the final desired bifunctional catalyst **PCI** was obtained as bright yellow crystals.

Motivated by positive reports on the performance of **2CzPN** as an energy transfer catalyst,[22] we envisioned a synthetic route toward a second bifunctional catalyst consisting of the chiral phosphoric acid backbone and **2CzPN** as the attached photocatalyst. To achieve this, a slightly different approach was used to access a brominated derivative of **2CzPN** (**9**), as depicted in Scheme 5. Although the synthesis of **9** was described in the literature,[23] our attempts at replicating the reported procedure for the synthesis of intermediate 8 were hindered by both incomplete reactivity and over addition of the carbazole, which presented challenging issues related to purification by column chromatography. Attempts to optimize the reaction conditions to give **8** in a quantitative yield were unsuccessful. By observing that the desired molecule **8** displayed lower solubilities in chloroform and DCM than the symmetric unwanted products (difluoro starting material and **2CzPN**), we were able to develop a new purification process to obtain pure **8** through multiple rounds of washes with chloroform/DCM.

Pure **9** was then submitted to the previously optimized conditions of the Suzuki coupling of **4**; namely a solvent mixture of 1,4-dioxane, water and DMF with Cs_2CO_3 as base and $Pd(PPh_3)_4$ as the palladium catalyst (Scheme 6A). Surprisingly, no desired cross-coupled product **10** was observed, and only what was assigned to be the monocoupled product was obtained. We hypothesized that this lack of biscoupling may be due to the increased steric hindrance of attaching the photocatalyst moiety directly at the carbazole, rather than by an additional benzylic linker as in the case of **5**. As such, an alternative route was explored, allowing a stepwise introduction of the steric bulk (Scheme 6B). First, the sterically less demanding 3-bromocarbazole was submitted to a Suzuki coupling yielding **11** in an excellent yield of 94%. We envisioned taking advantage of the reduced steric bulk surrounding the carbazole nitrogen to introduce the remainder of the photocatalyst through a nucleophilic aromatic coupling strategy. Gratifyingly, this coupling of **11** with aryl fluoride **8** was successful and produced desired intermediate **10** in 90% yield. It is noteworthy that the nucleophilic substitution leading to **10** was only achieved using NaH and not when using NaHMDS, the latter of which is often used in the synthesis of **2CzPN** or **4CzIPN**.[20a]

Unfortunately, the demethylation of **10** under the conditions described for the synthesis of photocatalyst **PCI** (1 M BBr_3 in DCM, 4.0 equiv) only led to the decomposition of **10**. Utilizing less harsh reaction conditions, such as lowering the temperature of the BBr_3 reaction to −78 °C before quenching at room temperature or using $AlCl_3$[24] in place of BBr_3, also failed to give the desired product and only resulted in the formation of decomposition products. The use of neat pyridine hydrochloride at 200 °C was next explored[25] but resulted in no conversion of the starting material 10. By doubling the equivalents of BBr_3 from 4 to 8 at a reaction temperature of −78 °C, while also quenching the reaction mixture at this low temperature, a new compound was obtained that was identified to be monodemethylated **10**. However, neither longer reaction times (1–6 h) nor more equivalents of BBr_3 were able to push the reaction to complete demethylation. Fortunately, it was found that using trimethylsilyl iodide[26] in dry deuterated chloroform followed by quenching with methanol overnight produced the desired doubly demethylated catalyst precursor **12** in a moderate yield of 61% (Scheme 7, step 1).

Targeting the formation of **PCII**, the free binaphthol **12** was then submitted to the same phosphorylation conditions as was used previously on **7** for the synthesis of **PCI**. However, in this case, it is worth mentioning that the resulting ^{31}P NMR spectrum showed three singlet phosphorus signals in proximity at 0.56, 0.76, and 0.92 ppm in DMSO-d_6. Conformational restrictions in **PCII** were suspected to be a potential cause of this observation. Therefore, high-temperature NMR studies in DMSO were carried out. However, these experiments proved inconclusive as heating the sample to 368 K (95 °C) did not result in coalescence of the signals. Further, neither different column chromatographic purification conditions nor recrystallization led to any observable change in the ratio of the signals in the NMR spectra (^1H and ^{31}P).

To confirm that none of these observed phosphorus peaks correspond to the intermediate phosphoryl chloride that is formed before hydrolysis to the desired phosphoric acid, the phosphoryl chloride was selectively synthesized and investigated by ^{31}P NMR[27] (see Supporting Information). The spectrum showed multiple peaks which were significantly shifted compared to the signals obtained for the acid (by ~2 ppm in $CDCl_3$), excluding the chloride as a source for the three signals. Since HRMS and ^1H NMR indicate that the desired phosphoric acid photocatalyst **PCII** was synthesized, we believe that **PCII** was obtained, and that the observed splitting is most likely caused by conformational effects.

A schematic view summarizing the synthesis of both **PCI** and **PCII** can be found in the Supporting Information.

PROOF-OF-CONCEPT REACTIONS

After the successful synthesis of the two novel bifunctional catalysts **PCI** and **PCII**, we first wanted to test their ability to induce chirality in known photochemical reactions. We were particularly interested in investigating whether the two catalysts can promote both asymmetric energy transfer and photoredox catalysis. For this purpose, the triplet energies and redox potentials of **PCI** and **PCII** were measured and compared to published values

of the corresponding parent compounds **4CzIPN** and **2CzPN** (Table 2; see Supporting Information for details).

Further, two proof-of-concept dual catalytic reactions were picked from the literature to evaluate the competency and performance of our catalysts. In both reactions, the original conditions relied upon a chiral phosphoric acid for asymmetric induction and a discrete photocatalyst for substrate activation.

The first investigated reaction was the energy transfer-catalyzed [2 + 2] cycloaddition depicted in Table 3 that was first published in a racemic fashion in 2020 by the group of Yoon.[30] In the achiral version, a ruthenium catalyst can only effectively excite the imidazole substrate **13** in the presence of the acid *p*-TsOH (20 mol %), as the acid cocatalyst facilitates the triplet energy transfer of the photocatalyst (Table 3, entries 1–4). A year later, the group published a chiral version of this reaction utilizing 1 mol % of $[Ir(Fppy)_2(dtbbpy)]PF_6$ as photocatalyst with 20 mol % of chiral BINOL-derived phosphoric acids **CPA-1** and **CPA-2** (entries 5–7).[31] At room temperature, their initial conditions utilizing **CPA-1** resulted in 72% yield with 37% enantiomeric excess (ee) and a diastereoselective ratio (dr) of 1:2 favoring the *trans–trans* **14** over the *trans–cis* product 14 (entry 5). Interestingly, when switching to the more acidic *N*-triflyl phosphoramide derivative of the chiral acid (**CPA-2**), they observed that no photocatalyst is needed at all and they can achieve similar yields via direct excitation with 20 mol % of acid in high ee (97%) and high, but reversed, dr (6:1 for the *trans–cis* product) when the temperature is decreased to −78 °C (entry 8).

When only 5 mol % of **PCI** was utilized with the same solvent system as reported by the Yoon group, an ee of 35% was achieved at room temperature (entry 9) with a yield of 70% while slightly favoring the *trans–trans* product **14** with a dr of 1:1.3 (*trans–cis:trans–trans*). **PCII** achieves similar yields (72%), albeit with a slightly lower enantioselectivity of 27% ee at room temperature but with better diastereoselectivity of 1:1.6 favoring the *trans–trans* product of **14** (entry 11). As higher enantiomeric values and better dr values were observed by the Yoon group when lowering the reaction temperature to −78 °C, we investigated the effects of low temperature for our catalysts as well (entries 10 and 12). We were delighted to find that upon lowering the temperature to −78 °C, both photocatalysts gave improved enantioselectivities, with **PCII** producing 65% ee with a simultaneously improved yield of 80% (entry 12). As observed in the original publication by the Yoon group, the diastereoselectivity also improved, now favoring the *trans–cis* product of **14** with a moderate dr of 3.8:1.

Highly motivated by these promising results indicating that **PCI** and **PCII** impart enantioselectivity in a visible-light mediated energy-transfer-catalyzed reaction, we wanted to further explore their performance as photoredox catalysts. To study this ability, we were especially interested in a recently published example of a chiral photoredox-catalyzed Minisci reaction (Table 4).[32] The reported example utilized 2 mol % of **4CzIPN** along with 10 mol % of a chiral phosphoric acid at 15 °C to construct chiral heterobiaryls **17** in good yields with excellent ee and diastereoselectivity (entry 1). We chose this example to test whether the novel bifunctional catalysts can replace the dual catalytic system and fulfill the role of both chiral phosphoric acid and photocatalyst in an enantioselective fashion in this

photoredox-catalyzed reaction. By subjecting both **PCI** and **PCII** to the literature reported reaction conditions, albeit at a slightly higher temperature (room temperature), we were delighted to find that without any optimization, an enantioselectivity of 21% with a yield of 33% was achieved with **PCI** (entry 4). Using only **4CzIPN** gave no product formation (entry 2), indicating that the phosphoric moiety of **PCI** is necessary for the reaction. Indeed, by adding 10 mol % racemic phosphoric acid *rac*-**PA**, racemic product **17** could be obtained with **4CzIPN** in low yields (entry 3).

This initial hit with **PCI** (entry 4) shows evidence of achieving chirality with our novel catalyst in reactions operating by a photoredox mechanism and we are optimistic that better enantioselectivity could be achieved by optimizing the reaction conditions for this specific catalyst.

CONCLUSION AND OUTLOOK

In summary, we have synthesized two novel catalysts that combine a chiral phosphoric acid with an organic, donor–acceptor cyanoarene-based photocatalyst moiety. Both are accessible in seven-step syntheses and all the synthetic challenges in accessing these catalysts have been overcome. In proof-of-concept reactions, the bifunctional catalysts have shown potential for both enantioselective energy transfer catalysis and photoredox catalysis. To explore the full potential of these novel catalysts, optimization studies need to be carried out to improve both yield and selectivity in the proof-ofconcept examples.

Going forward, a potential library of donor–acceptor cyanoarene-based chiral photocatalysts can be envisioned to tailor the photophysical properties of the catalysts to the reactions. A potential pathway to modulate the enantioselectivity of these catalysts is the introduction of only one photocatalyst unit (**PC**) and replacement of the second photocatalyst unit with a bulky group that better extends the chirality of the BINOL backbone into the substrate-binding pocket of the chiral phosphoric acid (Scheme 8-R^1). Further, enantioselectivity might be improved by increasing the acidity of the phosphoric acid through conversion to the *N*-triflyl phosphoramide (Scheme 8-R^2).[33] We believe that this new class of highly modular catalysts will help open new avenues of research in chiral photocatalysis.

EXPERIMENTAL SECTION

Materials and General Methods.

All reagents were purchased from commercial suppliers and used without further purification. Anhydrous solvents were obtained from Acros Organics in a AcroSeal bottle (“anhydrous”) or purified by passage through an activated alumina column under an argon atmosphere. Air sensitive reactions were performed in Schlenk vials or crimp capped vials under nitrogen (N_2) using plastic syringes and cannulas to transfer solvents or liquid reagents. The reactants of the photoreaction were weighed under air but degassed by three cycles of freeze pump thaw after addition of solvent to ensure complete exclusion of air. Analytical thin-layer chromatography (TLC) was performed using Merck silica gel 60 F254 TLC plates and visualized under UV or by staining with $KMnO_4$. Purification by flash column chromatography was performed on a Teledyne Isco CombiFlash. Enantiomeric

excess was determined by chiral HPLC using Daicel OD-H, OJ-H, IA, and IB columns (0.46 × 25 cm). All NMR spectra were recorded at room temperature unless otherwise noted using Bruker AV 600, Neo-500, AVB-400 and AVQ 400 spectrometers. These CoC-NMR instruments at UC Berkeley are funded in part by the NIH (S10OD024998). All chemical shifts are reported in δ-scale as parts per million [ppm] (multiplicity, coupling constant J, number of protons), relative to the solvent residual peaks as the internal standard ($CHCl_3$; δH = 7.268 ppm and δC = 77.16 ppm). Coupling constants J are given in Hertz [Hz]. Abbreviations used for signal multiplicity: ^{1}H NMR: b = broad, s = singlet, d = doublet, t = triplet, q = quartet, dd = doublet of doublets, ddd = doublet of doublet of doublets, dt = doublet of triplets, dq = doublet of quartets and m = multiplet. Optical rotations were determined using a PerkinElmer 241 polarimeter with a 10 cm glass cell and a sodium filter at the concentrations (g/100 mL) and temperatures noted. HRMS (high-resolution mass spectra) were measured at the QB3 mass spectra facility at the University of California, Berkeley. Photoreactions were performed using blue light with LT-1960 royal blue (blue, λ_{max} = 451 nm) as irradiation source in crimp capped vials in a water-cooled metal cooling block (distance approximately 1 cm) unless otherwise specified. The synthesis of literature reported compounds can be found in the Supporting Information.

For the determination of $E_{0-0}(S_1)$, UV/vis absorption spectra were recorded using a Shimdazu UV-2600i spectrophotometer and emission measurements were recorded using a Cary Eclipse fluorescence spectrophotometer (Varian).

For the determination of the triplet energy values $E_{0-0}(T_1)$, the following materials and methods were used: All steady state photophysical measurements were performed either in DCM (Merck, spectroscopic grade) or toluene (Merck, spectroscopic grade). The UV/vis absorption spectra were measured with a Cary 50 spectrometer (Agilent). The emission spectra as well as the emission decay of the samples were recorded at room temperature and at 77 K (using a quartz Dewar sample holder filled with liquid nitrogen) with a Fluorolog-3 fluorescence spectrometer (Horiba Jobin Yvon). The sample was placed in a 1.5 mm thin quartz capillary with an optical density at the excitation wavelength of ~1 over a 10 mm path length. The sample was excited at λ_{exc} = 380 nm and the emission recorded orthogonally to this.

For obtaining cyclic voltammetry (CV) data, the following materials and methods were used. Acetonitrile (MeCN) (99.9%, extra dry over molecular sieves) was obtained from Thermo Scientific. Tetrabutylammonium hexafluorophosphate ($TBAPF_6$; >99%, for electrochemical analysis) was obtained from MilliporeSigma, dried under high vacuum for 48 h at 75 °C, and transferred to a N_2-filled glovebox for storage and use. All electrochemical experiments were performed in a N_2-filled glovebox with an atmosphere <0.6 ppm oxygen and <0.1 ppm water. Electrolyte solutions were prepared in the glovebox by first drying the acetonitrile over freshly activated 3 Å molecular sieves for at least 24 h. Supporting electrolyte was then added and the solvent/electrolyte mixture was further dried for another 24 h before use. The resulting solvent/electrolyte mixtures were stored over the 3 Å molecular sieves in the glovebox. All potentials are reported relative to the ferrocene/ferrocenium couple (Fc/Fc^+), and this adjustment is made for each sample through the addition of a small amount of ferrocene reference. CV experiments were performed with a CH Instruments 760

bipotentiostat with a three-electrode electrochemical cell. A glassy carbon disk electrode (BASi, 3.0 mm diameter) was used as a working electrode, a Ag/Ag^+ electrode (5 mM $AgBF_4$ in 0.5 M $TBAPF_6$ in MeCN) sealed with a Coralpor frit was used as a non-aqueous quasi-reference electrode (BASi), and platinum mesh was used as a counter electrode. The glassy carbon electrode was polished outside the glovebox using alumina (MicroPolish II, Buehler) in Milli-Q water before being sonicated in Milli-Q water, dried with acetone, and brought into the glovebox. Unless otherwise indicated, all CV measurements were performed by dissolving the compound in stock 0.5 M $TBAPF_6$ in acetonitrile to give a concentration of 2.5 mM. E^0 values for the oxidation were approximated as follows: For both catalysts **PCI** and **PCII**, the oxidative couple was irreversible and caused significant passivation of the electrode, resulting in little to no reductive peaks in the return potential scans. To determine E^0 in these instances, the method of Vullev[34] was used that employs $E^{(i)}$, the inflection point of the anodic wave, as a good estimator for E^0. This value of $E^{(i)}$ is obtained from the first derivative of the anodic wave.

Preparation of Photocatalyst PCI.

3-(4-Bromobenzyl)-2,4,5,6-tetra(9H-carbazol-9-yl)benzonitrile (4). Small Scale with Blue LED (λ_{max} = 451 nm LED): A 5 mL crimp capped vial equipped with a magnetic stirring bar was charged with **4CzIPN** (47 mg, 60 μmol, 1.0 equiv), Cs_2CO_3 (78.2 mg, 240 μmol, 4.0 equiv), and 4-bromophenylacetic acid (51.6 mg, 240 μmol, 4.0 equiv). The mixture was degassed by three cycles of vacuum and nitrogen backfills before DMA (4 mL, not dry, 0.015 M) was added. The resulting mixture was stirred for 1 h under blue light irradiation (λ_{max} = 451 nm LED) through the plane bottom side of the vial (distance approximately 1 cm) at room temperature. The end of the reaction was visible by a color change from yellow to pink. For isolation, 12 reactions were first diluted with DCM and were then combined and washed once with water and once with brine. After drying over $MgSO_4$, the solvent was removed in vacuo in a 65 °C water bath to remove remaining DMA. The solid crude material was dissolved in DCM, and then equal amounts of EtOAC were added. Pure material crystallized over 48 h, and **4** was obtained as yellow solid (473 mg, 507 μmol, 70%).

Larger Scale with Kessil Lamp (λ_{max} = 440 nm): A 250 mL round-bottom flask equipped with a magnetic stirring bar was charged with **4CzIPN** (1.88 g, 2.38 mmol, 1.0 equiv), Cs_2CO_3 (3.12 g, 9.58 mmol, 4.0 equiv), and 4-bromophenylacetic acid (2.06 g, 9.58 mmol, 4.0 equiv). The mixture was degassed by three cycles of vacuum and nitrogen backfills before DMA (80 mL, not dry, 0.03 M) was added. The resulting mixture was stirred for 5 h under blue light irradiation (λ_{max} = 440 nm) with a Kessil Lamp (distance approximately 1 cm). After 5 h, the reaction was first diluted with DCM and then washed with water (3 times) and once with brine. After drying over $MgSO_4$, the solvent was removed in vacuo in a 65 °C water bath to remove remaining DMA. The solid crude material was dissolved in DCM (17 mL), and then equal amounts of EtOAC (17 mL) were added. Pure material crystallized out, and 4 was obtained as a yellow solid (1.60 g, 1.72 mmol, 72%): ^{1}H NMR (400 MHz, chloroform-*d*) δ 8.19 (d, J = 7.5 Hz, 2H), 7.72–7.60 (m, 6H), 7.48–7.39 (m, 4H), 7.31–7.23 (m, 4H), 7.11–6.99 (m, 10H), 6.91 (d, J = 8.2 Hz, 2H), 6.76 (t, J = 7.9 Hz, 2H), 6.67–6.58 (m, 2H), 6.58–6.54 (m, 2H), 5.77 (d, J = 8.4 Hz,

2H), 3.70 (s, 2H); $^{13}C\{^{1}H\}$ (126 MHz, chloroform-*d*) δ 144.9, 142.1, 140.9, 140.3, 140.1, 138.9, 138.7, 137.9, 136.4, 135.6, 130.9, 129.1, 127.0, 125.6, 125.6, 124.4, 124.3, 124.2, 123.8, 123.7, 121.6, 121.3, 121.3, 121.0, 120.4, 120.4, 120.3, 120.1, 119.5, 117.8, 112.7, 110.2, 110.1, 109.8, 109.1, 34.5 (*contains dimethylacetamide solvent peaks; carbazole-based photocatalysts tend to incorporate solvent molecules; contains ^{1}H-grease impurity*); HRMS (ESI^{+}) (*m*/*z*) $[M + Na]^{+}$ calcd for $C_{62}H_{38}N_5{}^{79}Br_1{}^{23}Na_1$ 954.2203; found 954.2207.

(R)-5,5′-(((2,2′-Dimethoxy-[1,1′-binaphthalene]-3,3′-diyl)bis(4,1-phenylene))bis(methylene))bis(2,3,4,6-tetra(9H-carbazol-9-yl)benzonitrile) (5).—A round-bottom flask equipped with a magnetic stirring bar was charged with **4** (1.92 g, 2.06 mmol 3.0 equiv), **2** (276 mg, 0.687 mmol, 1.0 equiv), Cs_2CO_3 (671 mg, 2.06 mmol, 3.0 equiv), and $Pd(PPh_3)_4$ (79 mg, 0.068 mmol, 10 mol %). The flask was degassed and backfilled with nitrogen three times before degassed solvent [dioxane (12.2 mL), water (4.1 mL) and DMF (7.5 mL)] was added. After stirring overnight at 85 °C (metal heating block), the reaction mixture was cooled to room temperature, diluted with 1 M HCl, and extracted with DCM twice. The combined organic phases were washed with water and brine, dried over $MgSO_4$, and the solvent was removed in vacuo. The crude reaction mixture was purified with flash column chromatography (0–70% DCM in hexanes) yielding 5 (589 mg, 0.292 mmol, 43%) as a yellow solid: ^{1}H NMR (600 MHz, chloroform-*d*) δ 8.22 (dd, *J* = 7.7, 2.5 Hz, 4H), 7.80 (d, *J* = 8.4 Hz, 2H), 7.71–7.61 (m, 12H), 7.50 (d, *J* = 9.1 Hz, 4H), 7.43 (td, *J* = 7.4, 6.9, 3.7 Hz, 4H), 7.38 (s, 2H), 7.36–7.32 (m, 2H), 7.28 (dd, *J* = 7.9, 3.6 Hz, 8H), 7.16 (ddd, *J* = 8.2, 6.8, 1.3 Hz, 2H), 7.10–6.98 (m, 22H), 6.91 (d, *J* = 8.1 Hz, 4H), 6.85 (d, *J* = 8.2 Hz, 4H), 6.78–6.73 (m, 4H), 6.65–6.59 (m, 4H), 6.07 (d, *J* = 8.2 Hz, 4H), 3.89 (s, 4H), 2.68 (s, 6H); $^{13}C\{^{1}H\}$ NMR (151 MHz, chloroform-*d*) δ 153.8, 145.4, 142.2, 141.1, 140.3, 140.2, 139.0, 138.8, 137.9, 136.8, 136.3, 136.1, 134.2, 133.4, 130.6, 128.7, 128.0, 127.5, 127.0, 126.2, 125.7, 125.6, 125.6, 125.5, 125.0, 124.4, 124.4, 124.3, 123.9, 123.7, 121.5, 121.5, 121.3, 121.2, 120.9, 120.9, 120.4, 120.3, 119.5, 117.7, 112.7, 110.2, 110.1, 110.0, 109.3, 60.5, 34.9 (*contains ^{1}H-grease impurity*); HRMS (ESI+) (*m*/*z*) $[M + Na]^{+}$ calcd for $C_{146}H_{92}O_2N_{10}{}^{23}Na_1$ 2039.7297; found 2039.7280.

(R)-5,5′-(((2,2′-Dihydroxy-[1,1′-binaphthalene]-3,3′-diyl)bis(4,1phenylene))bis(methylene))bis(2,3,4,6-tetra(9H-carbazol-9-yl)benzonitrile) (7).—A round-bottom flask equipped with a magnetic stirring bar was charged with **5** (558 mg, 276 μmol 1.0 equiv) and was degassed and backfilled with nitrogen three times before anhydrous DCM (2.1 mL) was added. The reaction mixture was cooled to 0 °C, and BBr_3 (1 M solution in DCM, 1.1 mL, 1.1 mmol, 4.0 equiv) was added dropwise. The reaction was stirred for 4 h at room temperature, cooled to 0 °C again, and quenched by slow addition of water. The mixture was diluted with DCM, and the aqueous phase was extracted with DCM three more times. The combined organic phases were dried over $MgSO_4$, and the solvent was removed in vacuo. The demethylated product **7** was obtained in quantitative yield (549 mg, 276 μmol) as a yellow solid without further purification: ^{1}H NMR (500 MHz, chloroform-*d*) δ 8.06 (d, *J* = 7.7 Hz, 4H), 7.65 (d, *J* = 8.1 Hz, 2H), 7.56–7.47 (m, 12H), 7.36 (t, *J* = 8.0 Hz, 4H), 7.28 (d, *J* = 8.1 Hz, 5H), 7.20–7.06 (m, 13H), 6.91 (ddt, *J* = 21.7, 18.2, 7.3 Hz, 22H), 6.81 (d, *J* = 8.1 Hz, 4H), 6.65 (d, *J* = 8.0 Hz, 4H), 6.61 (t, *J* = 6.5 Hz, 4H), 6.50 (t, *J* = 7.7 Hz, 4H), 5.94 (d, *J* = 7.9 Hz, 4H), 4.66 (s, 2H),

3.70 (s, 4H); $^{13}C\{^{1}H\}$ NMR (126 MHz, $CDCl_3$) δ 149.5, 145.4, 142.2, 141.0, 140.3, 140.2, 140.15, 139.0, 138.7, 138.7, 137.9, 136.5, 136.4, 135.2, 132.9, 131.0, 129.9, 129.2, 128.9, 128.3, 127.7, 127.0, 126.9, 125.6, 125.6, 124.4, 124.4, 124.3, 124.3, 124.2, 124.2, 123.8, 123.8, 123.6, 121.5, 121.5, 121.3, 121.2, 120.9, 120.4, 120.3, 119.5, 117.7, 113.0, 112.7, 110.2, 110.1, 109.9, 109.2, 34.9 (*the number of observed carbon peaks is higher than what would be expected based on symmetry, and it is believed to be due to rotameric and/or other conformational effects, that disrupt the symmetry; contains DCM solvent peaks; carbazole-based photocatalysts tend to incorporate solvent molecules; contains ^{1}H-grease impurity*); HRMS (ESI-) (*m*/*z*) $[M - H]^-$ calcd for $C_{144}H_{87}O_2N_{10}$ 1987.7019; found 1987.7009.

5,5′-((((11bR)-4-Hydroxy-4-oxidodinaphtho[2,1-d:1′,2′-f][1,3,2]dioxaphosphepine-2,6-diyl)bis(4,1-phenylene))bis(methylene))bis(2,3,4,6-tetra(9H-carbazol-9-yl)benzonitrile) (PCI).—A round-bottom flask equipped with a magnetic stirring bar was charged with **7** (509 mg, 256 μmol 1.0 equiv) and was degassed and backfilled with nitrogen three times before anhydrous pyridine (0.82 mL) was added. Phosphorus(V)oxychloride (48 μL, 0.51 mmol, 2.0 equiv) was added and the reaction mixture was stirred overnight at 95 °C (metal heating block) before the mixture was cooled to 0 °C and degassed water (0.8 mL) was added. Afterward, the mixture was heated up to 95 °C again and stirred overnight. The next day, the reaction mixture was cooled to room temperature, diluted with DCM and washed with 3 M HCl (×4). The solvent was removed in vacuo and the brownish solid was redissolved in hot acetonitrile. After letting the reaction mixture cool down to room temperature, it was allowed to stand undisrupted (approximately 2 days) until brown solid formed on the bottom of the flask. The clear yellow solution was filtered, and the solvent was once again removed in vacuo. The obtained yellow solid was further purified by flash column chromatography (0–3% methanol in DCM). Finally, pure catalyst **PCI** was obtained as yellow solid (300 mg, 146 μmol, 57%) by removing the solvent, redissolving it in DCM, washing it with 6 M HCl, and removing the solvent once again in vacuo: ^{1}H NMR (600 MHz, DMSO-d_6) δ 8.29 (dd, J = 7.7, 5.2 Hz, 4H), 8.16 (d, J = 8.1 Hz, 2H), 8.11 (d, J = 8.1 Hz, 2H), 8.04 (d, J = 8.2 Hz, 2H), 7.93 (dd, J = 21.1, 8.2 Hz, 4H), 7.85–7.63 (m, 20H), 7.47 (t, J = 7.6 Hz, 2H), 7.44–7.33 (m, 10H), 7.25–7.13 (m, 8H), 7.07 (dq, J = 15.7, 7.7 Hz, 6H), 7.02 (t, J = 7.5 Hz, 2H), 6.96 (dd, J = 21.7, 8.1 Hz, 4H), 6.82–6.71 (m, 12H), 6.16 (d, J = 7.9 Hz, 4H), 5.08 (s, 1H), 3.58 (s, 4H); $^{13}C\{^{1}H\}$ NMR (151 MHz, DMSO-d_6) δ 144.7, 144.6, 144.5, 142.7, 141.2, 140.2, 140.2, 139.3, 139.3, 138.7, 138.7, 138.5, 137.6, 135.2, 134.3, 133.2, 131.1, 131.0, 130.3, 128.6, 128.4, 126.6, 126.5, 125.9, 125.7, 125.2, 125.1, 124.9, 124.8, 123.8, 123.1, 123.0, 122.8, 122.7, 122.6, 122.4, 121.4, 120.8, 120.7, 120.7, 120.5, 120.1, 120.1, 119.9, 119.8, 119.7, 119.1, 117.5, 113.1, 111.8, 111.4, 111.4, 110.6, 110.6, 33.9 (*the number of observed carbon peaks is higher than what would be expected based on symmetry, and it is believed to be due to rotameric and/or other conformational effects, that disrupt the symmetry; contains ^{1}H-grease impurity*); ^{31}P NMR (243 MHz, DMSO-d_6) δ 0.57; HRMS (ESI+) (*m*/*z*) $[M + Na]^+$ calcd for $C_{144}H_{87}O_4N_{10}P_1{}^{23}Na_1$ 2073.6542; found 2073.6517; $[\alpha]_D{}^{25} = -89.0$ (c = 0.245, $CHCl_3$).

(R)-3,3′-(2,2′-Dimethoxy-[1,1′-binaphthalene]-3,3′-diyl)bis(9H-carbazole) (11).—A round-bottom flask equipped with a magnetic stirring bar was charged with 3-

bromocarbazole (1.48 g, 6.00 mmol 3.0 equiv), **2** (804 mg, 2.00 mmol, 1.0 equiv), Cs_2CO_3 (1.95 g, 6.00 mmol, 3.0 equiv), and $Pd(PPh_3)_4$ (0.23 g, 0.20 mmol, 10 mol %). The flask was degassed and backfilled with nitrogen three times before degassed solvent [dioxane (37.6 mL) and water (12.6 mL)] was added. After stirring overnight at 85 °C (oil bath), the reaction mixture was cooled to room temperature, diluted with 1 M HCl and extracted with DCM twice. The combined organic phases were washed with water and brine, dried over $MgSO_4$ and the solvent was removed in vacuo. The crude reaction mixture was purified with flash column chromatography (0–70% DCM in hexanes, then up to 100% DCM), yielding **11** (1.21 g, 1.87 mmol, 94%) as a white solid: ^{1}H NMR (500 MHz, chloroform-*d*) δ 8.52 (s, 2H), 8.13 (t, J = 4.0 Hz, 4H), 8.06 (s, 2H), 7.98 (d, J = 8.2 Hz, 2H), 7.87 (dd, J = 8.4, 1.7 Hz, 2H), 7.48–7.38 (m, 8H), 7.38–7.34 (m, 2H), 7.33–7.30 (m, 2H), 7.30–7.24 (m, 2H), 3.25 (s, 6H); ^{13}C{^{1}H} NMR (126 MHz, chloroform-*d*) δ 154.5, 140.0, 139.0, 135.9, 133.6, 131.1, 130.8, 130.4, 128.1, 127.7, 126.2, 126.2, 126.0, 126.0, 125.1, 123.6, 123.6, 121.2, 120.6, 119.7, 110.9, 110.5, 60.6 (*contains DCM solvent peaks; carbazole-based photocatalysts tend to incorporate solvent molecules*); HRMS (ESI-) (*m*/*z*) $[M - H]^-$ calcd for $C_{46}H_{31}O_2N_2$ 643.2391; found 643.2392.

(R)-5,5′-((2,2′-Dimethoxy-[1,1′-binaphthalene]-3,3′-diyl)bis(9Hcarbazole-3,9-diyl))bis(4-(9H-carbazol-9-yl)phthalonitrile) (10).—NaH (60% in oil, 148 mg, 3.70 mmol, 4.0 equiv) was added slowly to a stirred solution of **11** (596 mg, 0.924 mmol, 1.0 equiv) in dry THF (10 mL) under inert conditions. The reaction mixture was heated to 35 °C and stirred for 1 h before **8** (619 mg, 1.98 mmol, 2.1 equiv) was added. Afterward, it was stirred overnight at 35 °C (oil bath). The next day, the reaction mixture was cooled to room temperature and H_2O (0.7 mL) was added to quench excess NaH. The resulting mixture was then concentrated under reduced pressure, and the crude product was redissolved in DCM and washed with brine (2×). Purification by flash column chromatography (70–100% DCM in hexanes) yielded **10** (1.02 g, 0.831 mmol, 90%) as yellow solid: ^{1}H NMR (600 MHz, chloroform-*d*) δ 8.37–8.33 (m, 2H), 8.29 (t, J = 2.0 Hz, 2H), 8.19–8.15 (m, 2H), 7.93–7.83 (m, 6H), 7.76–7.71 (m, 2H), 7.71–7.66 (m, 2H), 7.49–7.43 (m, 2H), 7.42–7.36 (m, 2H), 7.28–7.01 (m, 20H), 7.00–6.95 (m, 4H), 2.98 (dd, J = 11.7, 4.4 Hz, 6H); ^{13}C{^{1}H} NMR (151 MHz, chloroform-*d*) δ 154.1, 154.1, 154.0, 154.0, 138.7, 138.7, 138.4, 138.3, 138.3, 138.3, 138.3, 138.2, 138.2, 137.6, 137.6, 135.6, 135.5, 134.9, 134.8, 134.8, 133.6, 133.5, 132.5, 132.4, 130.9, 130.9, 130.5, 130.5, 130.5, 129.1, 128.3, 128.1, 128.0, 127.7, 127.7, 127.7, 126.5, 126.4, 126.3, 126.3, 126.3, 126.3, 126.2, 126.1, 125.9, 125.9, 125.8, 125.8, 125.4, 125.2, 125.1, 124.5, 124.5, 124.4, 124.2, 124.2, 121.9, 121.9, 121.8, 121.8, 121.7, 121.3, 121.3, 121.2, 120.7, 120.7, 120.7, 120.5, 120.5, 120.4, 120.3, 120.3, 114.8, 114.7, 114.6, 109.2, 109.1, 109.1, 109.0, 109.0, 60.3, 60.3 (*the number of observed carbon peaks is higher than what would be expected based on symmetry, and it is believed to be due to rotameric and/or other conformational effects, that disrupt the symmetry*); HRMS (ESI +) (*m*/*z*) $[M + H]^+$ calcd for $C_{86}H_{51}O_2N_8$ 1227.4129; found 1227.4109.

(R)-5,5′-((2,2′-Dihydroxy-[1,1′-binaphthalene]-3,3′-diyl)bis(9H-carbazole-3,9-diyl))bis(4-(9H-carbazol-9-yl)phthalonitrile) (12).—A small Schlenk vial equipped with a magnetic stirring bar was charged with **10** (921 mg, 750 μmol, 1.0 equiv) and anhydrous deuterated chloroform (2.5 mL). Under nitrogen, trimethylsilyl

iodide (0.50 mL, 3.8 mmol, 5.0 equiv) was added and the reaction was heated to 60 °C (metal heating block) overnight. The next day, the mixture was filtered through a Celite pad and rinsed with chloroform and methanol was added. This mixture was left to stir another night at room temperature under nitrogen. After removing the solvent in vacuo, purification by column chromatography (DCM in hexane; 0 to 100%) and washing with hexane, **12** was obtained as yellow solid (551 mg, 459 μmol, 61%): ^{1}H NMR (600 MHz, chloroform-*d*) δ 8.26–8.23 (m, 4H), 8.16 (d, *J* = 4.5 Hz, 1H), 8.13 (d, *J* = 12.2 Hz, 1H), 7.93 (d, *J* = 5.6 Hz, 2H), 7.91–7.86 (m, 2H), 7.82–7.72 (m, 6H), 7.49–7.35 (m, 4H), 7.31 (q, *J* = 6.2, 4.2 Hz, 2H), 7.28–7.22 (m, 2H), 7.18–7.04 (m, 20H), 5.40–5.29 (m, 2H); ^{13}C{^{1}H} NMR (151 MHz, chloroform-*d*) δ 150.2, 150.1, 138.8, 138.4, 138.4, 138.4, 138.3, 137.9, 135.5, 135.5, 135.4, 133.0, 133.0, 131.3, 131.0, 130.6, 130.5, 129.5, 128.4, 127.9, 127.3, 126.5, 126.4, 126.3, 124.6, 124.4, 124.4, 124.3, 121.9, 121.8, 121.8, 121.6, 120.6, 120.5, 114.8, 114.8, 114.8, 114.6, 112.8, 112.8, 109.3, 109.1 (*contains ^{1}H-grease impurity and ethyl acetate solvent peaks; after initial purification, grease was observed in the product; to remove grease, the product was passed through a small silica plug with pure hexanes and then ethyl acetate; carbazole-based photocatalysts tend to incorporate solvent molecules*); HRMS (ESI+) (*m*/*z*) $[M + H]^+$ calcd for $C_{84}H_{47}O_2N_8$ 1199.3816; found 1199.3805; HRMS (ESI-) (*m*/*z*) $[M - H]^-$ calcd for $C_{84}H_{45}O_2N_8$ 1197.3671; found 1197.3666.

(4r,4′r)-5,5′-(((11bS)-4-Hydroxy-4-oxidodinaphtho[2,1-d:1′,2′-f]-[1,3,2]dioxaphosphepine-2,6-diyl)bis(9H-carbazole-3,9-diyl))bis(4-(9H-carbazol-9-yl)phthalonitrile) (PCII).—A round-bottom flask equipped with a magnetic stirring bar was charged with **12** (185 mg, 155 μmol, 1.0 equiv) and was degassed and backfilled with nitrogen three times before anhydrous pyridine (0.50 mL) was added. Phosphorus(V)oxychloride (29 μL, 0.31 mmol, 2.0 equiv) was added, and the reaction mixture was stirred overnight at 95 °C (metal heating block) before the mixture was cooled to 0 °C and degassed water was added. Afterward, the mixture was heated up to 95 °C again and stirred overnight. The next day, the reaction mixture was cooled to room temperature, diluted with DCM and washed with 3 M HCl (×4). The solvent was removed in vacuo, and the brownish solid was redissolved in hot acetonitrile. After letting the reaction mixture cool down to room temperature, it was allowed to stand undisrupted (approximately 2 days) until brown solid formed on the bottom of the flask. The clear yellow solution was filtered, and the solvent was once again removed in vacuo yielding **PCII** as yellow solid (127 mg, 100 μmol, 65%): ^{1}H NMR (600 MHz, DMSO-d_6) δ 8.88 (dd, *J* = 11.4, 6.0 Hz, 2H), 8.86–8.81 (m, 2H), 8.49 (d, *J* = 15.8 Hz, 1H), 8.44 (d, *J* = 15.0 Hz, 1H), 8.20 (d, *J* = 4.7 Hz, 1H), 8.17 (d, *J* = 3.7 Hz, 1H), 8.12 (dd, *J* = 8.3, 4.9 Hz, 2H), 8.00–7.88 (m, 6H), 7.85 (d, *J* = 8.5 Hz, 1H), 7.68–7.63 (m, 1H), 7.60 (dd, *J* = 8.6, 2.9 Hz, 1H), 7.57–7.48 (m, 5H), 7.38–7.32 (m, 2H), 7.28–7.13 (m, 10H), 7.10–7.01 (m, 6H), 7.03–6.94 (m, 2H); ^{13}C{^{1}H} NMR (151 MHz, DMSO-d_6) δ 145.4, 145.3, 145.3, 145.2, 145.2, 138.9, 138.8, 138.5, 138.4, 138.3, 138.1, 138.1, 138.1, 136.6, 136.5, 136.4, 136.4, 133.9, 133.8, 131.3, 131.1, 131.1, 130.9, 130.8, 130.0, 128.6, 128.2, 128.0, 126.6, 126.2, 126.1, 125.9, 125.8, 125.8, 125.7, 123.6, 123.4, 123.2, 122.3, 122.2, 121.9, 121.7, 121.1, 121.0, 120.3, 120.2, 120.1, 115.4, 115.1, 110.0, 110.0, 109.9, 109.6, 109.4 (*the number of observed carbon peaks is higher than what would be expected based on symmetry, and it is believed to be due to rotameric and/or other conformational effects, that disrupt the symmetry*); ^{31}P NMR (243

MHz, DMSO-d_6) δ 0.92, 0.76, 0.56 (*the number of observed phosphorus peaks is higher than what would be expected based on symmetry, and it is believed to be due to rotameric and/or other conformational effects, that disrupt the symmetry*); HRMS (ESI +) (*m*/*z*) [M + H]$^+$ calcd for $C_{84}H_{46}O_4N_8P_1$ 1261.3374; found 1261.3365; HRMS (ESI-) (*m*/*z*) [M – H]$^-$ calcd for $C_{84}H_{44}O_4N_8P_1$ 1259.3229; found 1259.3215; $[\alpha]_D^{25} = -336$ (*c* = 0.250, $CHCl_3$).

Supplementary Material

Refer to Web version on PubMed Central for supplementary material.

ACKNOWLEDGMENTS

We would like to thank Dr. Jacob S. Tracy (UC Berkeley) for measuring CV data and optical rotations, and Dr. Chin Ho Lee (UC Berkeley) for obtaining absorption and emission data of the photocatalysts at room temperature to estimate $E_{0-0}(S_1)$. We are grateful to Christina Graf (University of Regensburg) for supporting the emission data recording of the triplet emission at 77 K to estimate the triplet state energy $E_{0-0}(T_1)$. F.D.T. gratefully acknowledges the National Institutes of Health (R35 GM118190) for financial support. UC Berkeley's NMR facilities in the College of Chemistry (CoC-NMR) are supported in part by NIH S10OD024998. We thank Dr. Hasan Celik for spectroscopic assistance. This work was supported by the German Science Foundation (DFG, German Research Foundation; TRR 325-444632635). N.A. acknowledges a postdoc stipend at the University of Regensburg (Bayerisches Programm zur Realisierung der Chancengleichheit für Frauen in Forschung und Lehre und des Professorinnenprogramms des Bundes und der Länder III). A.B.R. would like to thank the Fonds der Chemischen Industrie (FCI) and the Studienstiftung des deutschen Volkes for financial support. We are also grateful to QB3/Chemistry Mass Spectrometry Facility (University of California, Berkeley) for HRMS analysis.

Data Availability Statement

The data underlying this study are available in the published article and its Supporting Information.

REFERENCES

(1). For reviews covering enantioselective photocatalysis, see: (a) Großkopf J; Kratz T; Rigotti T; Bach T. Enantioselective Photochemical Reactions Enabled by Triplet Energy Transfer. Chem. Rev 2022, 122, 1626–1653. [PubMed: 34227803] (b)Prentice C; Morrisson J; Smith AD; Zysman-Colman E. Recent developments in enantioselective photocatalysis. Beilstein J. Org. Chem 2020, 16, 2363–2441. [PubMed: 33082877] (c)Saha D. Catalytic Enantioselective Radical Transformations Enabled by Visible Light. Chem. Asian J 2020, 15, 2129–215. [PubMed: 32463981] (d)Silvi M; Melchiorre P. Enhancing the potential of enantioselective organocatalysis with light. Nature 2018, 554, 41–49. [PubMed: 29388950] (e)Zou Y-Q; Hormann FM; Bach T. Iminium and enamine catalysis in enantioselective photochemical reactions. Chem. Soc. Rev 2018, 47, 278–290. [PubMed: 29155908] (f)Brimioulle R; Lenhart D; Maturi MM; Bach T. Enantioselective Catalysis of Photochemical Reactions. Angew. Chem., Int. Ed 2015, 54, 3872–3890.

(2). Brenninger C; Jolliffe JD; Bach T. Chromophore Activation of α,β-Unsaturated Carbonyl Compounds and Its Application to Enantioselective Photochemical Reactions. Angew. Chem., Int. Ed 2018, 57, 14338–14349.

(3). Burg F; Bach T. Lactam Hydrogen Bonds as Control Elements in Enantioselective Transition-Metal-Catalyzed and Photochemical Reactions. J. Org. Chem 2019, 84, 8815–8836. [PubMed: 31181155]

(4). (a)Leverenz M; Merten C; Dreuw A; Bach T. Lewis Acid Catalyzed Enantioselective Photochemical Rearrangements on the Singlet Potential Energy Surface. J. Am. Chem. Soc 2019, 141, 20053–20057. [PubMed: 31814393] (b)Stegbauer S; Jandl C; Bach T. Enantioselective Lewis Acid Catalyzed ortho Photocycloaddition of Olefins to Phenanthrene9-carboxaldehydes. Angew. Chem.Int. Ed 2018, 57, 14593–14596.(c)Poplata S; Bach T. Enantioselective

Intermolecular [2 + 2] Photocycloaddition Reaction of Cyclic Enones and Its Application in a Synthesis of (−)-Grandisol. J. Am. Chem. Soc 2018, 140, 3228–3231. [PubMed: 29458250] (d)Brimioulle R; Bauer A; Bach T. Enantioselective Lewis Acid Catalysis in Intramolecular [2 + 2] Photocycloaddition Reactions: A Mechanistic Comparison between Representative Coumarin and Enone Substrates. J. Am. Chem. Soc 2015, 137, 5170–5176. [PubMed: 25806816] (e)Brimioulle R; Bach T. Enantioselective Lewis Acid Catalysis of Intramolecular Enone [2 + 2] Photocycloaddition Reactions. Science 2013, 342, 840–843. [PubMed: 24233720] (f)Guo H; Herdtweck E; Bach T. Enantioselective Lewis Acid Catalysis in Intramolecular [2 + 2] Photocycloaddition Reactions of Coumarins. Angew. Chem., Int. Ed 2010, 49, 7782–7785.

(5). (a)Daub ME; Jung H; Lee BJ; Won J; Baik M-H; Yoon TP Enantioselective [2 + 2] Cycloadditions of Cinnamate Esters: Generalizing Lewis Acid Catalysis of Triplet Energy Transfer. J. Am. Chem. Soc 2019, 141, 9543–9547. [PubMed: 31145856] (b)Miller ZD; Lee BJ; Yoon TP Enantioselective Crossed Photocycloadditions of Styrenic Olefins by Lewis Acid Catalyzed Triplet Sensitization. Angew. Chem., Int. Ed 2017, 56, 11891–11895.(c)Blum TR; Miller ZD; Bates DM; Guzei IA; Yoon TP Enantioselective photochemistry through Lewis acid–catalyzed triplet energy transfer. Science 2016, 354, 1391–1395. [PubMed: 27980203] (d)Amador AG; Sherbrook EM; Yoon TP Enantioselective Photocatalytic [3 + 2] Cycloadditions of Aryl Cyclopropyl Ketones. J. Am. Chem. Soc 2016, 138, 4722–4725. [PubMed: 27015009] (e)Ruiz Espelt L; McPherson IS; Wiensch EM; Yoon TP Enantioselective Conjugate Additions of α-Amino Radicals via Cooperative Photoredox and Lewis Acid Catalysis. J. Am. Chem. Soc 2015, 137, 2452–2455. [PubMed: 25668687] (f)Du J; Skubi KL; Schultz DM; Yoon TP A Dual-Catalysis Approach to Enantioselective [2 + 2] Photocycloadditions Using Visible Light. Science 2014, 344, 392–396. [PubMed: 24763585]

(6). (a)Huang X; Meggers E. Asymmetric Photocatalysis with Biscyclometalated Rhodium Complexes. Acc. Chem. Res 2019, 52, 833–847. [PubMed: 30840435] (b)Steinlandt PS; Zuo W; Harms K; Meggers E. BisCyclometalated Indazole Chiral-at-Rhodium Catalyst for Asymmetric Photoredox Cyanoalkylations. Chem.Eur. J 2019, 25, 15333–15340. [PubMed: 31541505] (c)Kuang Y; Wang K; Shi X; Huang X; Meggers E; Wu J. Asymmetric Synthesis of 1,4-Dicarbonyl Compounds from Aldehydes by Hydrogen Atom Transfer Photocatalysis and Chiral Lewis Acid Catalysis. Angew. Chem., Int. Ed 2019, 58, 16859–16863.(d)Huang X; Lin J; Shen T; Harms K; Marchini M; Ceroni P; Meggers E. Asymmetric [3 + 2] Photocycloadditions of Cyclopropanes with Alkenes or Alkynes through Visible-Light Excitation of Catalyst-Bound Substrates. Angew. Chem., Int. Ed 2018, 57, 5454–5458.(e)Huang X; Quinn TR; Harms K; Webster RD; Zhang L; Wiest O; Meggers E. Direct Visible-Light-Excited Asymmetric Lewis Acid Catalysis of Intermolecular [2 + 2] Photocycloadditions. J. Am. Chem. Soc 2017, 139, 9120–9123. [PubMed: 28644024] (f)Huo H; Harms K; Meggers E. Catalytic, Enantioselective Addition of Alkyl Radicals to Alkenes via Visible-Light-Activated Photoredox Catalysis with a Chiral Rhodium Complex. J. Am. Chem. Soc 2016, 138, 6936–6939. [PubMed: 27218134] (g)Huang X; Webster RD; Harms K; Meggers E. Asymmetric Catalysis with Organic Azides and Diazo Compounds Initiated by Photoinduced Electron Transfer. J. Am. Chem. Soc 2016, 138, 12636–12642. [PubMed: 27577929] (h)Huo H; Wang C; Harms K; Meggers E. Enantioselective, Catalytic Trichloromethylation through VisibleLight-Activated Photoredox Catalysis with a Chiral Iridium Complex. J. Am. Chem. Soc 2015, 137, 9551–9554. [PubMed: 26193928]

(7). Cauble DF; Lynch V; Krische MJ Studies on the Enantioselective Catalysis of Photochemically Promoted Transformations: “Sensitizing Receptors” as Chiral Catalysts. J. Org. Chem 2003, 68, 15–21. [PubMed: 12515455]

(8). (a)Maturi MM; Bach T. Enantioselective Catalysis of the Intermolecular [2 + 2] Photocycloaddition between 2-Pyridones and Acetylenedicarboxylates. Angew. Chem., Int. Ed 2014, 53, 7661–7664.(b)Müller C; Bauer A; Maturi MM; Cuquerella MC; Miranda MA; Bach T. Enantioselective Intramolecular [2 + 2]-Photocycloaddition Reactions of 4-Substituted Quinolones Catalyzed by a Chiral Sensitizer with a Hydrogen-Bonding Motif. J. Am. Chem. Soc 2011, 133, 16689–16697. [PubMed: 21955005] (c)Müller C; Bauer A; Bach T. LightDriven Enantioselective Organocatalysis. Angew. Chem., Int. Ed 2009, 48, 6640–6642.(d)Bauer A; Westkämper F; Grimme S; Bach T. Catalytic enantioselective reactions driven by photoinduced electron transfer. T. Nature 2005, 436, 1139–1140.

(9). Alonso R; Bach T. A Chiral Thioxanthone as an Organocatalyst for Enantioselective [2 + 2] Photocycloaddition Reactions Induced by Visible Light. Angew. Chem., Int. Ed 2014, 53, 4368–4371.

(10). Pecho F; Zou Y-Q; Gramüller J; Mori T; Huber SM; Bauer A; Gschwind RM; Bach T. A Thioxanthone Sensitizer with a Chiral Phosphoric Acid Binding Site: Properties and Applications in Visible Light-Mediated Cycloadditions. Chem.Eur. J 2020, 26, 5190–5194. [PubMed: 32065432]

(11). (a)Kratz T; Steinbach P; Breitenlechner S; Storch G; Bannwarth C; Bach T. Photochemical Deracemization of Chiral Alkenes via Triplet Energy Transfer. J. Am. Chem. Soc 2022, 144, 10133–10138. [PubMed: 35658423] (b)Takagi R; Tanimoto T. Enantioselective [2 + 2] photocycloaddition of quinolone using a C_1-symmetric chiral phosphoric acid as a visible-light photocatalyst. Org. Biomol. Chem 2022, 20, 3940–3947. [PubMed: 35506886] (c)Lyu J; Leone M; Claraz A; Allain C; Neuville L; Masson G. Syntheses of new chiral chimeric photoorganocatalysts. RSC Adv. 2021, 11, 36663–36669. [PubMed: 35494356] (d)Pecho F; Sempere Y; Gramüller J; Hörmann FM; Gschwind RM; Bach Enantioselective [2 + 2] Photocycloaddition via Iminium Ions: Catalysis by a Sensitizing Chiral Brønsted Acid. J. Am. Chem. Soc 2021, 143, 9350–9354. [PubMed: 34156845] (e)Nikitas NF; Gkizis PL; Kokotos CG Thioxanthone: a powerful photocatalyst for organic reactions. Org. Biomol. Chem 2021, 19, 5237–5253. [PubMed: 34047729] (f)Lyu J; Claraz A; Vitale MR; Allain C; Masson G. Preparation of Chiral Photosensitive Organocatalysts and Their Application for the Enantioselective Synthesis of 1,2-Diamines. J. Org. Chem 2020, 85, 12843–12855. [PubMed: 32957790] (g)Rigotti T; Casado-Sánchez A; Cabrera S; Pérez-Ruiz R; Liras M; de la Peña O'Shea VA; Aleman J. A Bifunctional Photoaminocatalyst for the Alkylation of Aldehydes: Design, Analysis, and Mechanistic Studies. ACS Catal. 2018, 8, 5928–5940.(h)Mayr F; Mohr L-M; Rodriguez E; Bach T. Synthesis of Chiral ThioureaThioxanthone Hybrids. Synthesis 2017, 49, 5238–5250.(i)Ding W; Lu L-Q; Zhou Q-Q; Wei Y; Chen J-R; Xiao W-J Bifunctional Photocatalysts for Enantioselective Aerobic Oxidation of β-Ketoesters. J. Am. Chem. Soc 2017, 139, 63–66. [PubMed: 28001382]

(12). Some recent initial work has been done on modifying the photochemical properties of nonchiral thioxanthone-based triplet sensitizers: (a) Elliott LD; Kayal S; George MW; Booker-Milburn K. Rational Design of Triplet Sensitizers for the Transfer of Excited State Photochemistry from UV to Visible. J. Am. Chem. Soc 2020, 142, 14947–14956. For tuning of the absorption spectra, see: [PubMed: 32786778] (b)Iyer A; Clay A; Jockusch S; Sivaguru J. Evaluating brominated thioxanthones as organo-photocatalysts. Phys. Org. Chem 2017, 30, e3738.

(13). (a)Speckmeier E; Fischer TG; Zeitler K. A Toolbox Approach To Construct Broadly Applicable Metal-Free Catalysts for Photoredox Chemistry: Deliberate Tuning of Redox Potentials and Importance of Halogens in Donor–Acceptor Cyanoarenes. J. Am. Chem. Soc 2018, 140, 15353–15365. [PubMed: 30277767] (b)Luo J; Zhang J. Donor– Acceptor Fluorophores for Visible-Light-Promoted Organic Synthesis: Photoredox/Ni Dual Catalytic C(sp3)–C(sp2) Cross-Coupling. ACS Catal. 2016, 6, 873–87.

(14). Shang T-Y; Lu L-H; Cao Z; Liu Y; He W-M; Yu B. Recent advances of 1,2,3,5-tetrakis(carbazol-9-yl)-4,6-dicyanobenzene (4CzIPN) in photocatalytic transformations. Chem. Commun 2019, 55, 5408–5419.

(15). (a)Huang S; Zhang Q; Shiota Y; Nakagawa T; Kuwabara K; Yoshizawa K; Adachi C. Computational Prediction for Singlet-and Triplet-Transition Energies of Charge-Transfer Compounds. J. Chem. Theory Comput 2013, 9, 3872–3877. [PubMed: 26592382] (b)Uoyama H; Goushi K; Shizu K; Nomura H; Adachi C. Highly efficient organic light-emitting diodes from delayed fluorescence. Nature 2012, 492, 234–238. [PubMed: 23235877]

(16). Bryden MA; Zysman-Colman E. Organic thermally activated delayed fluorescence (TADF) compounds used in photocatalysis. Chem. Soc. Rev 2021, 50, 7587–7680. [PubMed: 34002736]

(17). TADF molecules in energy transfer catalysis: (a) Hojo R; Polgar AM; Hudson ZM Thermally Activated Delayed Fluorescence Sensitizers As Organic and Green Alternatives in Energy-Transfer Photocatalysis. ACS Sustainable Chem. Eng 2022, 10, 9665–9678.(b)Lu J; Pattengale B; Liu Q; Yang S; Shi W; Li S; Huang J; Zhang J. Donor-Acceptor Fluorophores for Energy-Transfer-Mediated Photocatalysis. J. Am. Chem. Soc 2018, 140, 13719–13725. [PubMed: 30277771]

(18). Lingenfelter DS; Helgeson RC; Cram DJ Host-guest complexation. 23. High chiral recognition of amino acid and ester guests by hosts containing one chiral element. J. Org. Chem 1981, 46, 393–406.

(19). Simonsen KB; Gothelf KV; Jørgensen KA A Simple Synthetic Approach to 3,3'-Diaryl BINOLs. J. Org. Chem 1998, 63, 7536–7538. [PubMed: 11672412]

(20). (a)Grotjahn S; König B. Photosubstitution in Dicyanobenzene-based Photocatalysts. Org. Lett 2021, 23, 3146–3150. [PubMed: 33821659] (b)Donabauer K; Maity M; Berger AL; Huff GS; Crespi S; König B. Photocatalytic carbanion generation – benzylation of aliphatic aldehydes to secondary alcohols. Chem. Sci 2019, 10, 5162–5166. [PubMed: 31183069]

(21). (a)Uraguchi D; Terada M. Chiral Brønsted Acid-Catalyzed Direct Mannich Reactions via Electrophilic Activation. J. Am. Chem. Soc 2004, 126, 5356–5357. [PubMed: 15113196] (b)Uraguchi D; Sorimachi K; Terada M. Enantioselective Mannich-Type Reaction Catalyzed by a Chiral Brønsted Acid. J. Am. Chem. Soc 2004, 126, 11804–11805. [PubMed: 15382910]

(22). Rolka AB; König B. Dearomative Cycloadditions Utilizing an Organic Photosensitizer: An Alternative to Iridium Catalysis. Org. Lett 2020, 22, 5035–5040. [PubMed: 32567316]

(23). Gan S; Hu S; Li X-L; Zeng J; Zhang D; Huang T; Luo W; Zhao Z; Duan L; Su S-J; Tang BZ Heavy Atom Effect of Bromine Significantly Enhances Exciton Utilization of Delayed Fluorescence Luminogens. ACS Appl. Mater. Interfaces 2018, 10, 17327–17334. [PubMed: 29722959]

(24). Bhalodi EH; Shah VR; Butcher RJ; Bedekar AV Synthesis and Study of Photophysical Properties of 6,12-Dicyano-9-oxa[7]helicene. ChemistrySelect 2021, 6, 13514–13519.

(25). Kulkarni PP; Kadam AJ; Mane RB; Desai UV; Wadgaonkar PP Demethylation of Methyl Aryl Ethers using Pyridine Hydrochloride in Solvent-free Conditions under Microwave Irradiation. J. Chem. Res. (S) 1999, 394–395.

(26). Jung ME; Lyster MA Quantitative dealkylation of alkyl ethers via treatment with trimethylsilyl iodide. A new method for ether hydrolysis. J. Org. Chem 1977, 42, 3761–3764.

(27). Romanov-Michailidis F; Romanova-Michaelides M; Pupier M; Alexakis A. Enantioselective Halogenative Semi-Pinacol Rearrangement: Extension of Substrate Scope and Mechanistic Investigations. Chem.Eur. J 2015, 21, 5561–5583. [PubMed: 25711981]

(28). (a)Romero NA; Nicewicz DA Organic Photoredox Catalysis. Chem. Rev 2016, 116, 10075–10166. [PubMed: 27285582] (b)McNaught A; Wilkinson A. Gibbs Energy of Photoinduced Electron Transfer. In IUPAC Compendium of Chemical Terminology, 2nd ed. (the "Gold Book"); Nič M, Jirát J, Košata B, Jenkins A, Eds.; Blackwell Scientific Publications: Oxford, 1997.

(29). Pavlishchuk VV; Addison AW Conversion constants for redox potentials measured versus different reference electrodes in acetonitrile solutions at 25 °C. Inorg. Chim. Acta 2000, 298, 97–102.

(30). Sherbrook EM; Jung H; Cho D; Baik M-H; Yoon TP Brønsted acid catalysis of photosensitized cycloadditions. Chem. Sci 2020, 11, 856–861.

(31). Sherbrook EM; Genzink MJ; Park B; Guzei IA; Baik M-H; Yoon TP Chiral Brønsted acid-controlled intermolecular asymmetric [2 + 2] photocycloadditions. Nat. Commun 2021, 12, 5735. [PubMed: 34593790]

(32). The shown example is based on: (a) Liang D; Chen J-R; Tan L-P; He Z-W; Xiao W-J Catalytic Asymmetric Construction of Axially and Centrally Chiral Heterobiaryls by Minisci Reaction. J. Am. Chem. Soc 2022, 144, 6040–6049. For previous and pioneering work on this topic, see: [PubMed: 35322666] (b)Proctor RSJ; Davis HJ; Phipps RJ Catalytic enantioselective Minisci-type addition to heteroarenes. Science 2018, 360, 419–422. [PubMed: 29622723]

(33). Nakashima D; Yamamoto H. Design of Chiral N-Triflyl Phosphoramide as a Strong Chiral Brønsted Acid and Its Application to Asymmetric Diels–Alder Reaction. J. Am. Chem. Soc 2006, 128, 9626–9627. [PubMed: 16866505]

(34). Espinoza EM; Clark JA; Soliman J; Derr JB; Morales M; Vullev VI Practical Aspects of Cyclic Voltammetry: How to Estimate Reduction Potentials When Irreversibility Prevails. J. Electrochem. Soc 2019, 166, H3175–H3187.

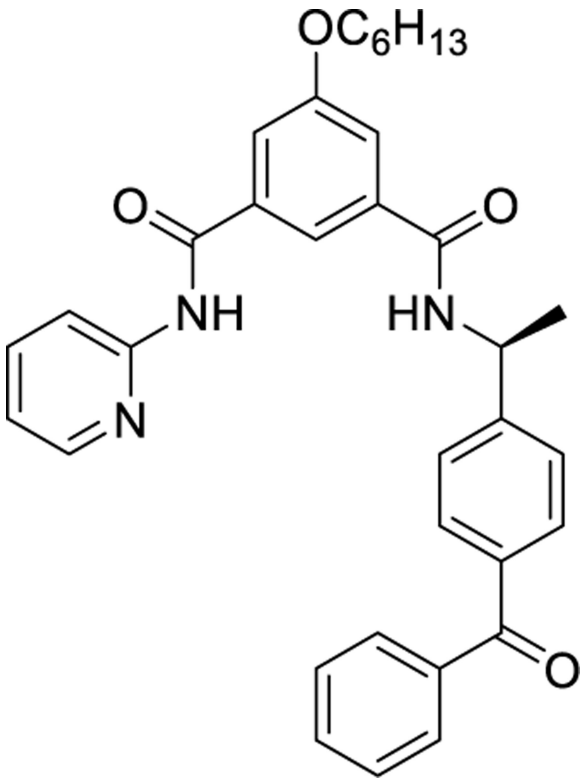

Figure 1.
Structure of the chiral hydrogen bonding catalyst introduced by Krische.[7]

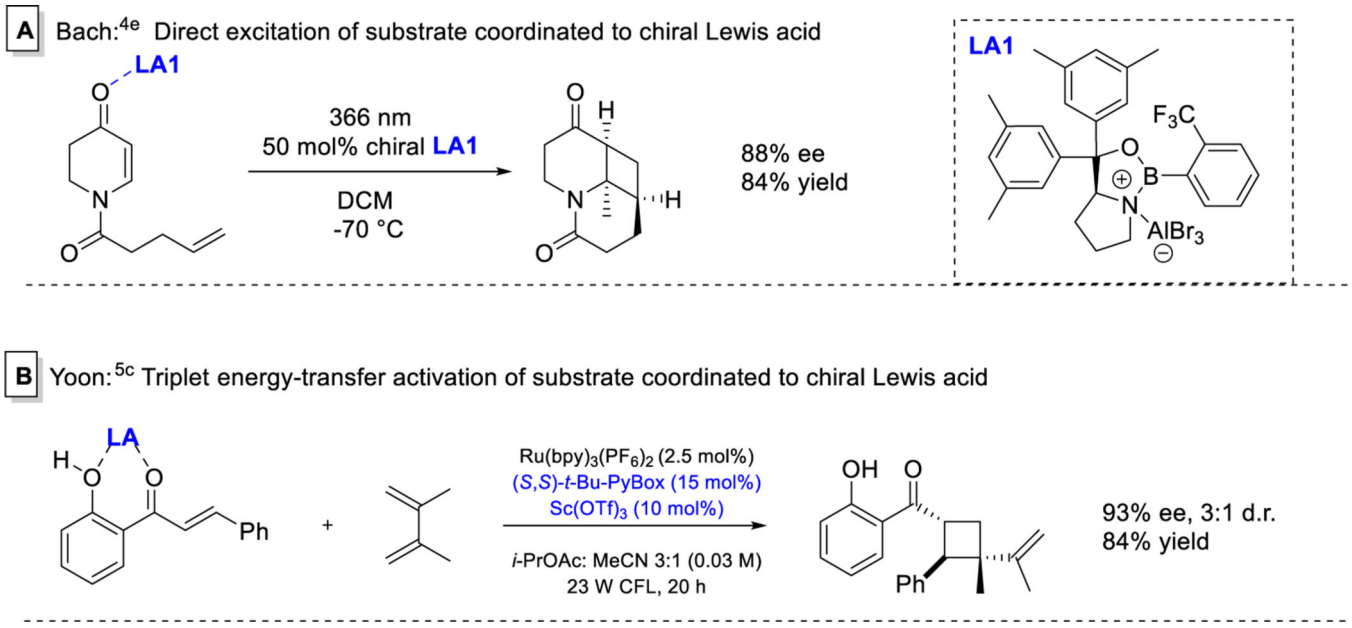

Scheme 1.
Chiral Lewis Acid Catalysts for Enantioselective Photocatalysis

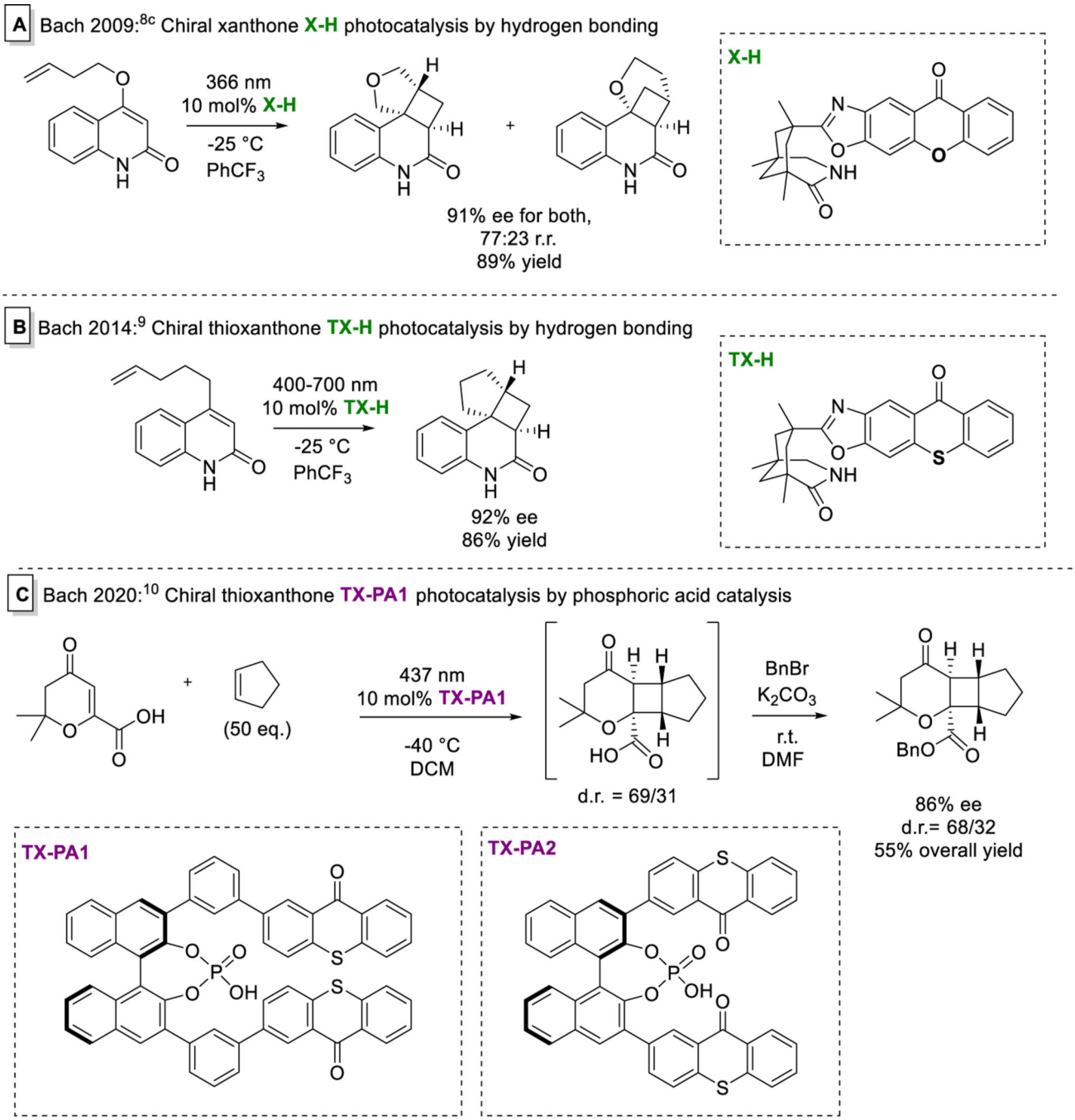

Scheme 2.

Chiral Xanthone and Thioxanthone Catalysts for Enantioselective Photocatalysis

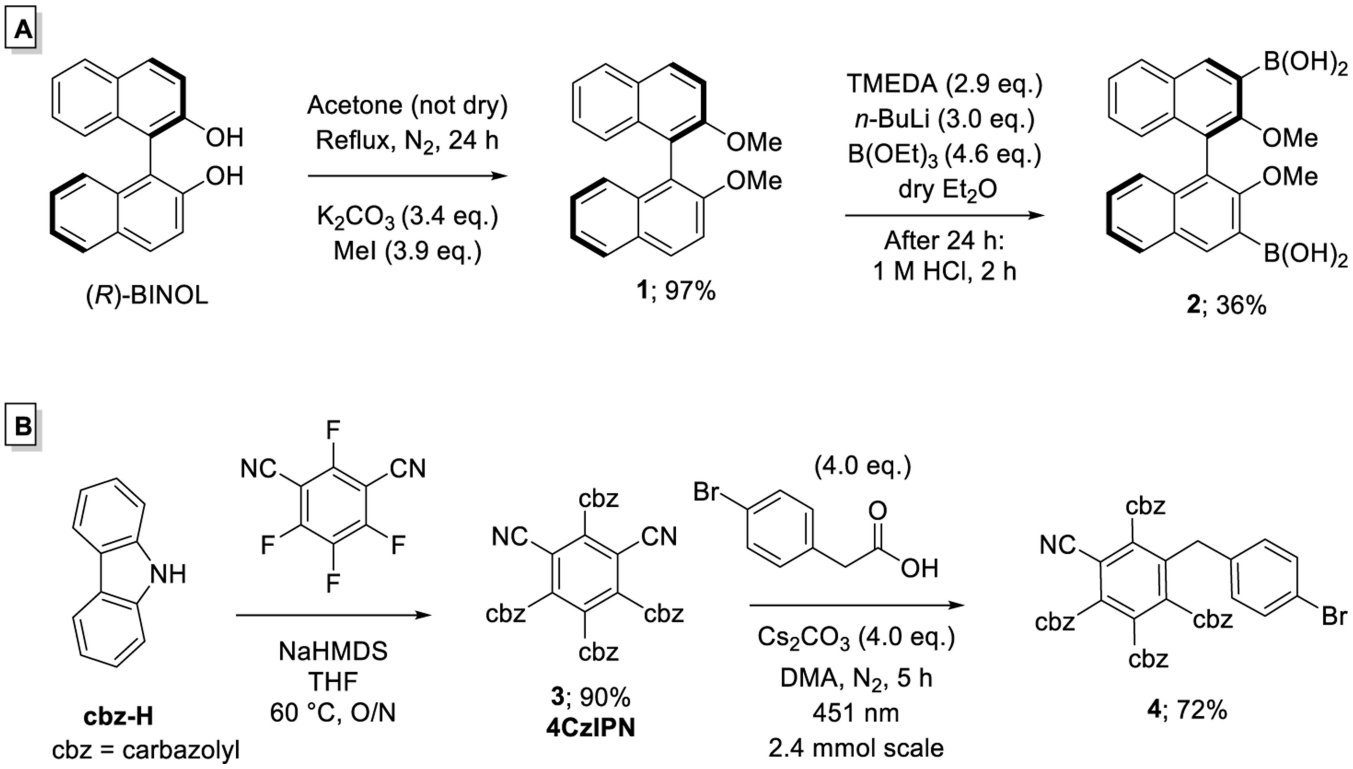

Scheme 3.

Synthesis of Chiral Boronic Acid 2 (A) and Brominated 4CzIPN Derivative 4 (B)

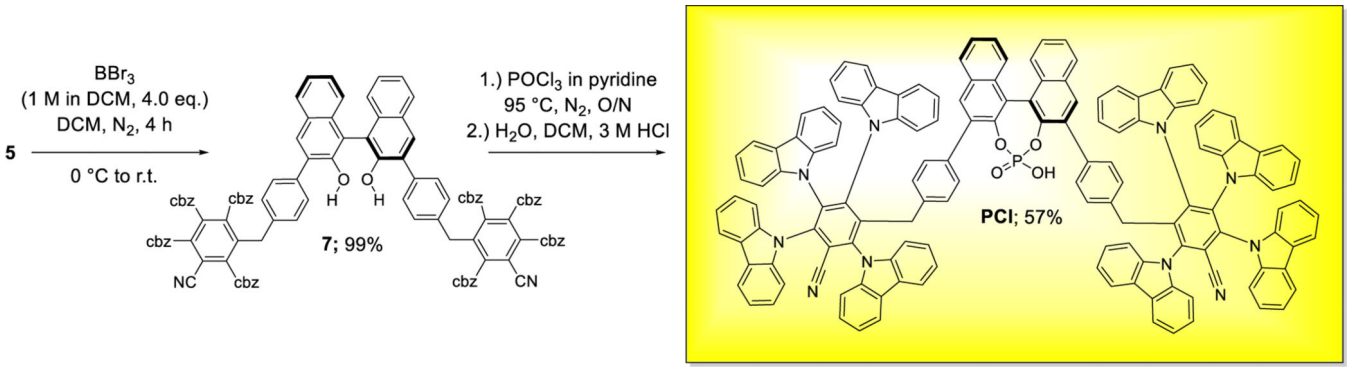

Scheme 4.
Synthesis of PCI via Demethylation of 5 to 7

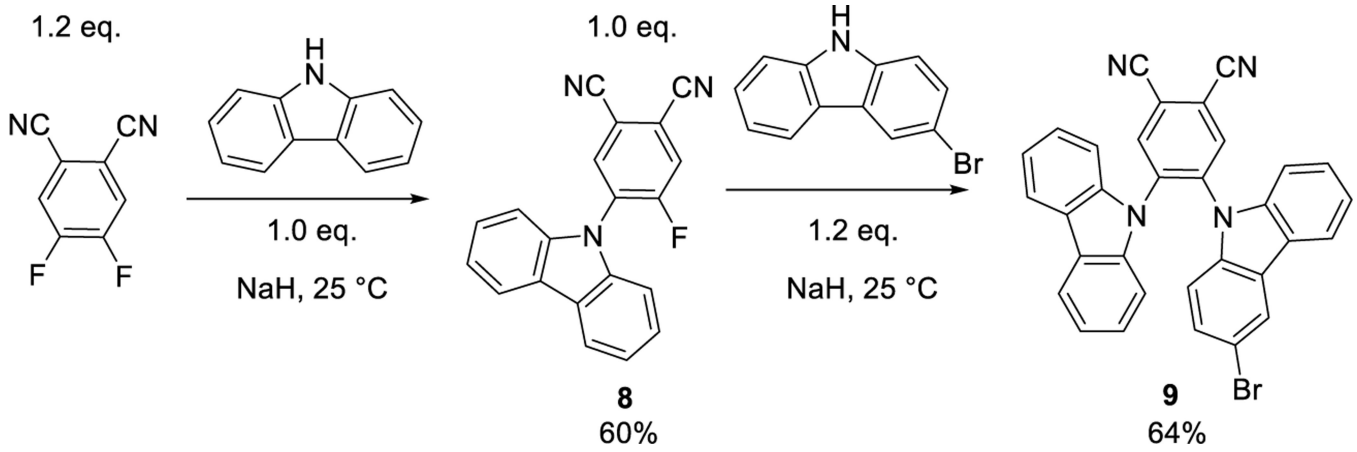

Scheme 5.
Synthesis of Brominated 2CzPN Derivative 9 and Monosubstituted 8

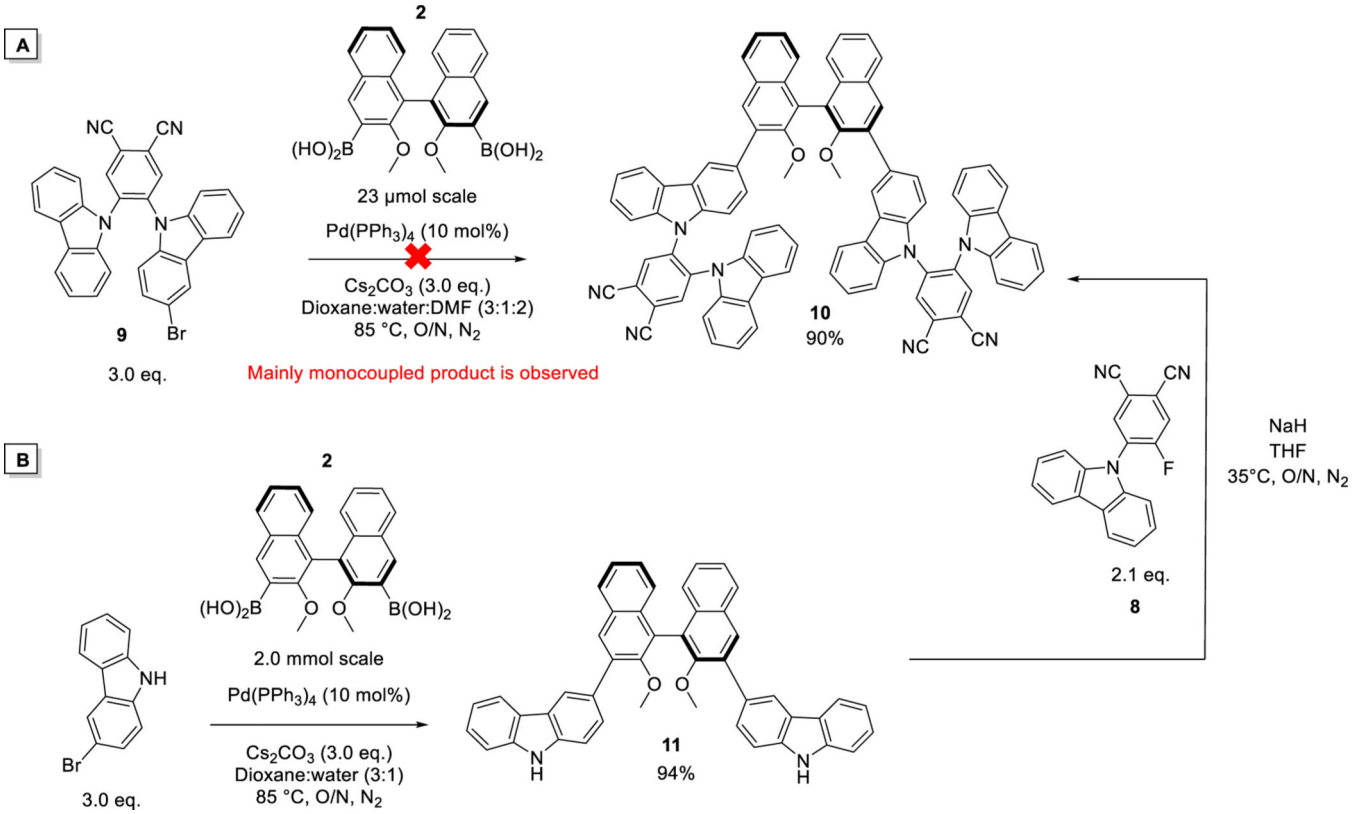

Scheme 6.
Strategies to Access 10

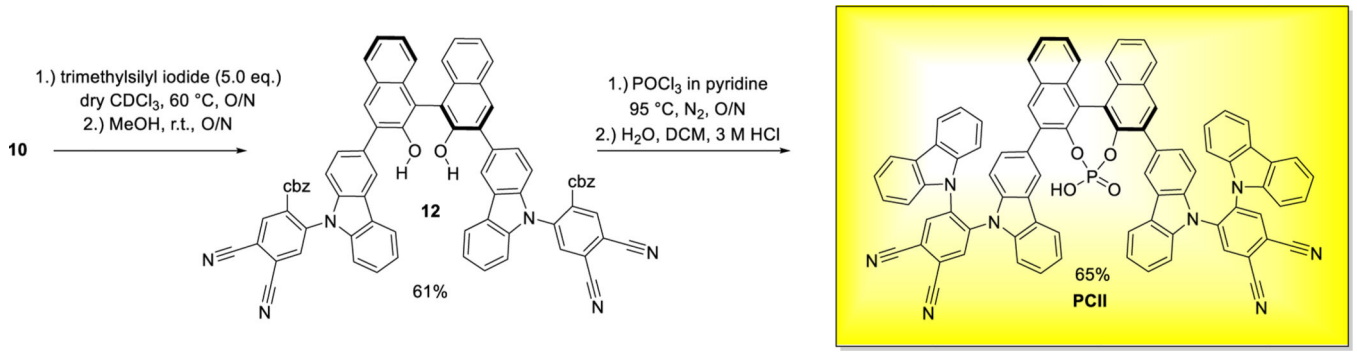

Scheme 7.
Synthesis of PCII via Demethylation of 10 to 12

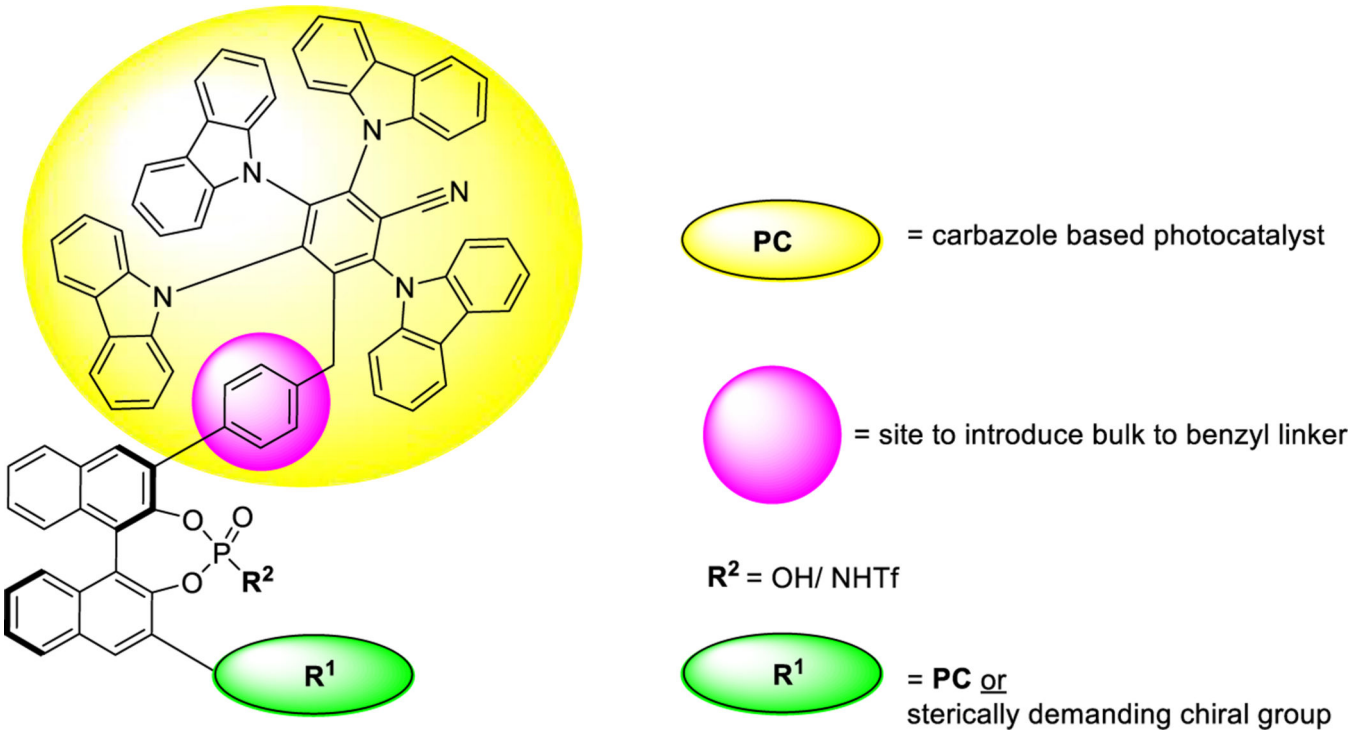

Scheme 8.

Possible Points of Modulating the Catalyst's Structure to Build up a Chiral Library

J Org Chem. Author manuscript; available in PMC 2024 May 19.

Table 1.

Optimization of the Cross-Coupling of 4 with 2

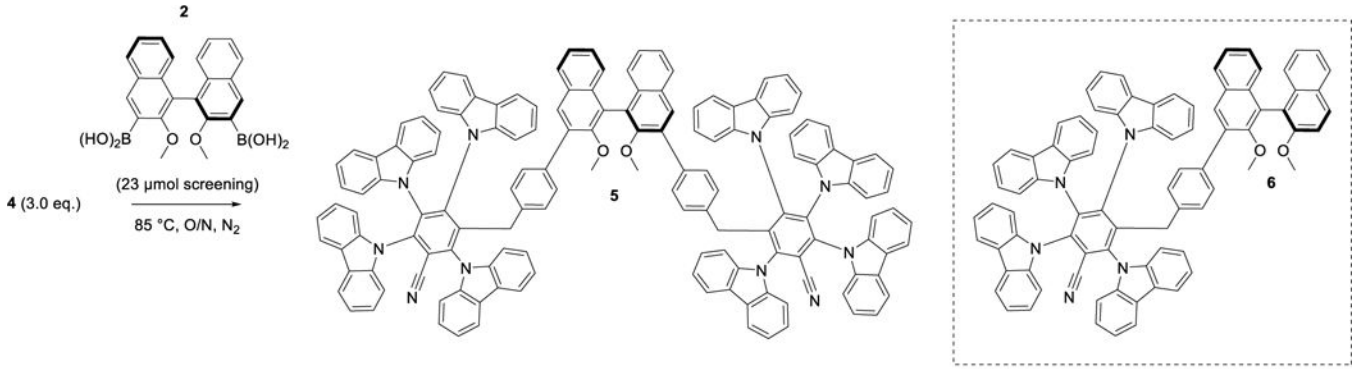

Entry	Pd (10 mol%)	Base (3.0 eq.)	Solvent	Yield (%)
1	$Pd(PPh_3)_4$	$Ba(OH)_2{\cdot}8H_2O$	1,4-dioxane: water (3:1)	26[a]
2	$Pd(PPh_3)_4$	$Ba(OH)_2{\cdot}8H_2O$	1,4-dioxane: water: DMF (3:1:2)	42[a]
3	$Pd(PPh_3)_4$	$Ba(OH)_2{\cdot}8H_2O$	water: DMF (3:1)	27[a]
4	[c]$Pd(PPh_3)_4$	$Ba(OH)_2{\cdot}8H_2O$	1,4-dioxane: water: DMF (3:1:2)	35[b]
5	$Pd(PPh_3)_4$	[d]$Ba(OH)_2{\cdot}8H_2O$	1,4-dioxane: water: DMF (3:1:2)	37[b]
6	$Pd(PPh_3)_4$	Na_2CO_3	1,4-dioxane: water: DMF (3:1:2)	20[a]
7	**$Pd(PPh_3)_4$**	**Cs_2CO_3**	**1,4-dioxane: water: DMF (3:1:2)**	**45[b]**

[a] ^{1}H NMR yield using mesitylene as internal standard.

[b] Isolated yield.

[c] Catalyst loading of 20 mol %.

[d] 10.0 equiv instead of 3.0 equiv.

Table 2.

Redox Potentials and Triplet Energies of Novel Catalysts and Their Parent Compounds[a]

PCI	$E_{1/2}(P^{\bullet+}/*P)$[b]	$E_{1/2}(*P/P^{\bullet-})$[b]	$E_{1/2}(P^{\bullet+}/P)$	$E_{1/2}(P/P^{\bullet-})$	E_{0-0}(Si) [eV]	E_{0-0}(Ti) [eV][e]	ref
PCI	−1.51	+1.20	+1.37[c]	−1.68[c]	2.88[d]	2.49[f], 2.51[g]	
4CzIPN	−1.04	+1.35	+1.52	−1.21	2.56	2.53[f]	13, 15
PCII	−1.46	+1.37	+1.37[c]	−1.46[c]	2.83[d]	2.48[f,g]	
2CzPN	−1.30	+1.32	+1.47	−1.45	2.77	2.63[f]	13, 15

[a] All potentials are given in volts vs saturated calomel electrode (SCE) and were measured in MeCN at room temperature.

[b] Calculated according to $E_{1/2}(P^{\bullet+}/*P) = (E_{1/2}(P^{\bullet+}/P) - E_{0-0}(S_1))$ and $E_{1/2}(*P/P^{\bullet-}) = (E_{0-0}(S_1) + E_{1/2}(P/P^{\bullet-}))$.[28]

[c] Using ferrocene as internal standard and converted to SCE according to $Fc^{+}/Fc \rightarrow$ SCE: +0.380 V.[29]

[d] Estimated from the point of intersection of the excitation and emission spectra at room temperature.

[e] Estimated from the highest slope of the longest wavelength edge of the corresponding emission spectrum recorded at 77 K.

[f] Measured in toluene.

[g] Measured in DCM.

J Org Chem. Author manuscript; available in PMC 2024 May 19.

Table 3.

Energy-Transfer-Catalyzed [2 + 2]-Cycloaddition as a Proof-of-Concept Reaction

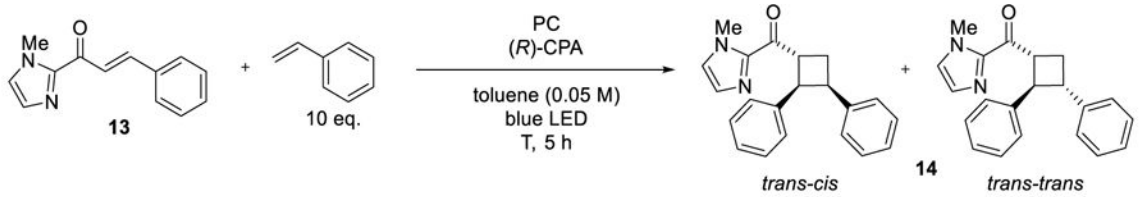

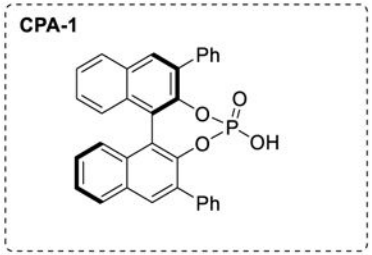

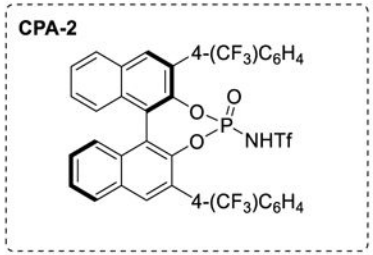

Entry	PC	CPA[c]	Temp. T (°C)	Yield (%)[e]	ee (%)	d.r.[i]
1[a]	None	None	r.t.	0	nd[f]	-
2[a]	$Ru(bpy)_3Cl_2$ (2.5 mol%)	None	r.t.	11	nd[f]	1:2
3[a]	None	*p*-TsOH	r.t.	Trace	nd[f]	-
4[a]	$Ru(bpy)_3Cl_2$ (2.5 mol%)	*p*-TsOH	r.t.	75	nd[f]	1:2
5[b]	$Ir(Fppy)_2(dtbbpy)PF_6$ (1 mol%)	CPA-1	r.t.	72	37[g]	1:2
6[b]	$Ir(Fppy)_2(dtbbpy)PF_6$ (1 mol%)	CPA-1	-78	83	81[g]	4:1
7[b]	$Ir(Fppy)_2(dtbbpy)PF_6$ (1 mol%)	CPA-2	-78	74	95[g]	7:1
8[b]	None	CPA-2	-78	71	97[g]	6:1
9	PCI (5 mol%)	None	r.t.[d]	70	35[h]	1:1.3
10	PCI (5 mol%)	None	-78	63	54[h]	2.2:1
11	PCII (5 mol%)	None	r.t.[d]	72	27[h]	1:1.6
12	PCII (5 mol%)	None	-78	80	65[h]	3.8:1

[a]Entries and values from the original publication of the Yoon group.[30] Reaction was carried out in MeCN for 16 h with nonchiral acids.

[b]Entries and values from the original publication of the Yoon group.[31]

[c]20 mol % was used.

[d]Reactions were run overnight.

[e]Yield determined by ^{1}H NMR analysis of crude reaction mixture with phenanthrene as internal standard.

[f]Not determined.

[g]Enantiomeric excess of the major diastereomer determined by chiral HPLC.

[h]Enantiomeric excess of the *trans–cis* diastereomer determined by chiral HPLC.

[i]Diastereomeric ratios determined by ^{1}H NMR analysis of crude reaction mixture.

Table 4.

Photoredox-Catalyzed Minisci Reaction As a Proof-of-Concept Reaction

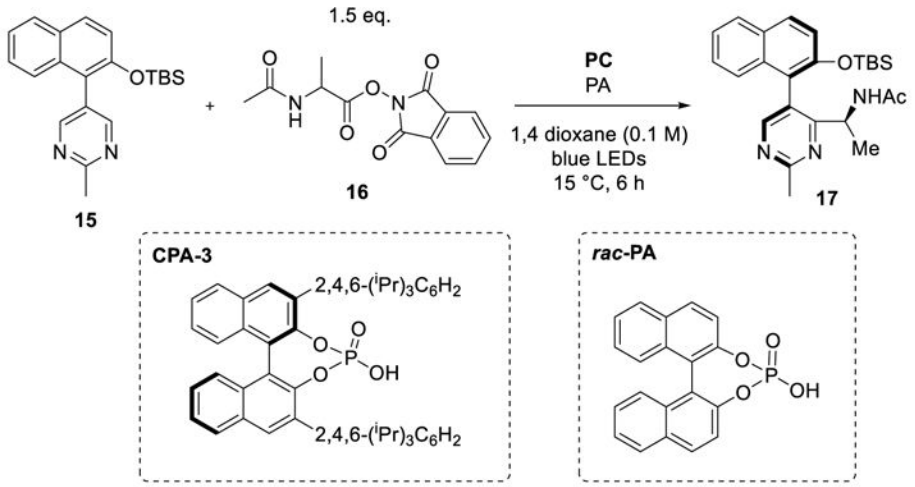

Entry	PC	PA	Yield (%)[c]	ee (%)[d]	d.r.[f]
1[a]	4CzIPN (2 mol%)	CPA-3 (10 mol%)	64	>99	>19:1
2[b]	4CzIPN (10 mol%)	None	-	-	-
3[b]	4CzIPN (2 mol%)	*rac*-PA (10 mol%)	17	-	nd[e]
4[b]	PCI (10 mol%)	None	33	21	>19:1
5[b]	PCII (10 mol%)	None	13	14	>10:1[g]

[a] Entries and values from the publication of the Xiao group.[32a]

[b] Reactions were run overnight at room temperature.

[c] ^{1}H NMR analysis with 1,3,5-trimethoxybenzene as the internal standard.

[d] Enantiomeric excess was determined by chiral HPLC.

[e] Not determined.

[f] Diastereomeric ratios determined by ^{1}H NMR analysis.

[g] Due to low conversion and formation of undesired and unidentifiable products, we were unable to define a dr greater than 10:1 with high levels of confidence.